Tuning the topological state of a helical atom chain via a Josephson phase

A. A. Bespalov

Institute for Physics of Microstructures, Russian Academy of Sciences, 603950 Nizhny Novgorod, GSP-105, Russia
and National Research Lobachevsky State University of Nizhny Novgorod, 603950 Nizhny Novgorod, Russia

(Received 12 July 2022; revised 1 September 2022; accepted 26 September 2022; published 7 October 2022)

By solving the Bogoliubov-de Gennes equations, we study the quasiparticle spectrum of a magnetic atom chain placed inside a short constriction-type Josephson junction. A helical magnetic order of the atomic spins is assumed, so that a topologically nontrivial state with Majorana edge modes at the ends of the chain can appear. It is found that in the presence of a nonzero Josephson phase the subgap spectrum of an infinite chain consists of four branches (Shiba bands). This spectrum is almost certainly gapped if the atomic spins form a coplanar spiral. The Majorana number of the given system is calculated analytically. It is demonstrated that a Josephson phase shift can be used to drive the system into a topologically nontrivial state and to tune the size of the topological gap. The spatial structure of Majorana edge modes is studied as well. We generalize the effective model based on discrete Bogoliubov-de Gennes equations developed by Pientka *et al.* for a bulk superconductor to the case of a Josephson junction. Using these discrete equations, the wave functions of Majorana zero modes are calculated analytically for a coplanar atomic spin spiral with arbitrary pitch. The wave functions exhibit an intermediate asymptotic behavior with a nonexponential fall-off with distance from the edge of the atomic chain.

DOI: 10.1103/PhysRevB.106.134503

I. INTRODUCTION

The concept of topological quantum computation is based on performing operations with qubits via braiding of non-Abelian anyons—quasiparticles whose physical permutations are noncommutative [1,2]. In condensed matter physics, one of the simplest examples of such anyon is the so-called Majorana zero mode (MZM). As demonstrated by Alexei Kitaev, MZMs appear at the ends of 1D and quasi-1D topological superconductors [3]. In a sufficiently long, but finite 1D wire, two such modes can be combined into an ordinary Bogoliubov quasiparticle state with near-zero energy localized at both ends of the wire.

Topological superconductivity appears to be not easy to obtain. One of the first and most promising practical proposals to construct a 1D topological superconductor was based on using semiconducting wires with spin-orbit interaction, proximity-induced superconductivity and a strong Zeeman field (obtained either by applying a magnetic field or from intrinsic exchange interaction) [4,5]. There is mounting experimental evidence for the presence of MZMs in such systems—see Ref. [6] for a review. Later it was found that the spin-orbit interaction can be excluded, if the Zeeman field is noncollinear, e.g. a spiral magnetic order is present [7,8]. In fact, even proximitized wires are not necessary: it was demonstrated that topological superconductivity may occur in the vicinity of magnetic atom chains with noncollinear magnetic order, and the phase diagram of superconducting systems with such chains has been studied in a number of papers [9–21]. It was argued that helical magnetic order should appear spontaneously in magnetic chains coupled to a superconductor due to different mechanisms [11–13,16,22–27], which may result in a topologically nontrivial phase.

Technically, atomic chains on metallic surfaces can be created by means of single-atom manipulation using the tip of a scanning tunneling microscope. Generally, the artificially created magnetic chains exhibit collinear magnetic order, however, in some cases a spiral order occurs [28–31] (presumably, due to the Dzyaloshinskii-Moriya interaction between atomic spins). In Ref. [31], signatures of MZMs were found at the ends of a Fe chain deposited on superconducting Re.

In 1D topological superconductor networks, braiding can be performed by locally changing the topological state of the system [32]. In nanowire-based systems [4,5], this can be accomplished by tuning the chemical potential (via gate electrodes) or the magnetic field. These mechanisms are not that efficient in systems based on helical magnetic chains (though a magnetic field can induce a phase bias, whose impact is discussed below), so that alternative experimental knobs are necessary. It has been demonstrated for various systems that a superconducting phase bias, which is usually related with a supercurrent flow, can act as such a knob [15,33–46]. The influence of a uniform supercurrent on the quasiparticle spectrum of a helical atom chain placed inside a bulk superconductor has been studied by Röntynen and Ojanen [15]. The authors considered the dilute limit, $k_F a \gg 1$, where k_F is the Fermi wave number and a is the distance between magnetic atoms, and the limit of deep Yu-Shiba-Rusinov (YSR) states [47–49], so that the energies of quasiparticles hosted by each atom are much smaller than the bulk superconducting gap Δ_0. It was found that the supercurrent allows to tune the topological state of the system, e.g. to switch from a topologically trivial to a nontrivial state.

An important limitation of the mentioned approach [15] to tune the properties of a helical atom chain is that the gradient of the phase θ_S of the superconducting order parameter can

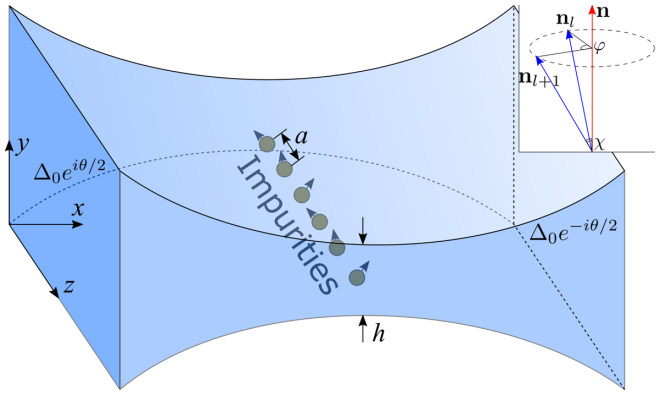

FIG. 1. Josephson junction of the constriction type with a chain of point impurities. On the left and right, the order parameter in the superconducting banks is shown ($\Delta = \Delta_0 e^{\pm i\theta/2}$). (Inset) Scheme explaining the meaning of the angles φ and χ.

be only of the order of or smaller than ξ^{-1}, where ξ is the coherence length—for $|\nabla\theta_S| \sim \xi^{-1}$, the supercurrent is of the order of the depairing current. For this reason, in Ref. [15], the limit $|\nabla\theta_S| \ll \xi^{-1}$ was analyzed, so that the suppression of the superconducting gap could be neglected. To consider the effect of larger phase gradients, in the present paper we study a somewhat different setup, namely, a magnetic atom chain placed inside a short weak link of the constriction type, as shown in Fig. 1. The idea behind this setup is as follows. The YSR states induced by each atom (impurity) in a bulk superconductor are generally not deep (the energy may be of the order of Δ_0). In the magnetic chain, these states hybridize to form Shiba bands. In the dilute limit ($k_F a \gg 1$), these bands are typically narrow, and the helical chain is in a topologically trivial state: the atoms can be moved infinitely far apart without closing the spectral gap. In the constriction geometry, the Josephson phase difference θ can be used to significantly tune the energy of the YSR states: the energy may be shifted by a value of the order of Δ_0 [50]. Hence, by applying a phase bias it may be possible to close the spectral gap and to drive the system into a topologically nontrivial state (when the gap reopens). Our calculations prove that this is indeed possible in a wide range of parameters.

Within the Bogoliubov-de Gennes equations formalism, we analyze the spectral properties of quasiparticle states localized at the helical chain in our system. We consider chains with arbitrary pitch and tilt angles, as well as arbitrary energies of YSR states. The magnetic atoms are described as point scatterers with scattering phases $\alpha_\uparrow$ and $\alpha_\downarrow$ for "spin-up" and "spin-down" electrons, respectively. In preceding papers, for simplicity the case $\alpha_\uparrow = -\alpha_\downarrow$ was considered. Here, we study the more general case when $\alpha_\uparrow$ and $\alpha_\downarrow$ are independent. For some simplifications, we consider the limit $a \ll \xi$.

We start by calculating the spectrum of impurity-induced states in an infinite helical chain. We find that in our system in the presence of a Josephson phase difference four Shiba bands appear, as opposed to two bands found in preceding papers for a uniform superconductor [14,15,18]. For a nonplanar spin helix, a gapless phase exists for some range of phases θ, while for a planar helix the gapless phase is absent, similarly to Refs. [14,18] (the same situation takes place in the case of a bulk supercurrent flowing perpendicular to the atom chain [15]). Next, we study the phase diagram of the chain. The Majorana number is calculated, and it is found that it does not depend on the tilt angle χ of the spin helix. It is demonstrated that the topological state of the system and the size of the topological gap can be tuned by varying the phase θ.

Finally, we study the structure of the MZMs. Previously, for a uniform bulk superconductor, it was found using numerical calculations that in a long chain with a planar helix and in the limit $k_F a \gg 1$ and $\xi \to \infty$ the wave function Ψ of a MZM falls off with distance s from the edge of the chain as

$$\Psi \sim \frac{1}{s \ln^{\mu}(s/a)} \tag{1}$$

with $\mu = 2$ [14]. Later [51], for a limited range of parameters this result was confirmed analytically using an approximate solution of the two-band model derived in Ref. [14]. Here, we derive a generalization of the mentioned model for our system, which includes a Josephson phase difference θ. We find an analytical solution for the wave function of the MZM in the case of a planar helix for an arbitrary pitch of the helix and arbitrary θ. We demonstrate that for $\theta \neq 0$ Eq. (1) is still applicable, but the exponent μ depends on θ.

The paper is organized as follows. In Sec. II, the physical model is described in detail, and the problem of calculating the quasiparticle spectrum is cast in the form of a system of discrete linear equations. In Sec. III, the spectrum of an infinite atomic chain is calculated. In Sec. IV A the phase diagram of the chain is studied. In Sec. IV B, the wave functions of low-energy quasiparticle states are analyzed numerically and analytically. In Sec. V, possible experimental implementations are discussed. The main results are summarized in the conclusion. Most analytical calculations can be found in the appendices.

II. PHYSICAL MODEL AND BASIC EQUATIONS

We will consider a three-dimensional Josephson junction with a smooth constriction as a weak link, as shown in Fig. 1. For our analysis, it does not matter whether superconductivity is suppressed in the region of the weak link or not. The key assumptions that we will use are that the width h of the constriction and its characteristic length in the x direction are much smaller than the bulk coherence length $\xi = \hbar v_F/(\pi\Delta_0)$, where v_F is the Fermi velocity of the superconducting material. The condition $h \ll \xi$ allows for significant variations of the order parameter's phase in the weak-link region on a scale that is much smaller than ξ in the clean limit (we use such a gauge that the vector potential can be neglected in the vicinity of the junction)—see Sec. III D 2 in Ref. [52]. Thus we are dealing with a short weak link. The order parameter's phase in the left and right superconducting banks is $\theta/2$ and $-\theta/2$, respectively.

Inside the junction, there is a chain of magnetic atoms oriented along the z axis. The atoms are identical, and their spins exhibit a spiral order. We assume that apart from the magnetic atoms, the superconductor contains no defects in the region of the junction with a spatial extent of several coherence lengths.

We will calculate the energies and spatial structures of impurity-induced states in our system within the formalism of the Bogoliubov-de Gennes (BdG) equations:

$$\left\{\check{\tau}_z[H_0(\mathbf{r})+U(\mathbf{r})]+\mathbf{J}(\mathbf{r})\check{\boldsymbol{\sigma}}+\begin{pmatrix}0 & \Delta(\mathbf{r})\\ \Delta^*(\mathbf{r}) & 0\end{pmatrix}_N\right\}\Psi=E\Psi, \tag{2}$$

where the star * denotes complex conjugation,

$$\Psi(\mathbf{r})=\begin{pmatrix}u_\uparrow(\mathbf{r})\\ u_\downarrow(\mathbf{r})\\ v_\uparrow(\mathbf{r})\\ v_\downarrow(\mathbf{r})\end{pmatrix} \tag{3}$$

is a vector in the space that is the tensor product of spin and Nambu spaces, $\uparrow$ and $\downarrow$ are spin projection indices, $\check{\tau}_z$ is a Pauli matrix in Nambu space, $\check{\boldsymbol{\sigma}}=(\check{\sigma}_x,\check{\sigma}_y,\check{\sigma}_z)$ is a vector composed of Pauli matrices, $U(\mathbf{r})$ is the electric potential, $\mathbf{J}(\mathbf{r})$ is the exchange field, $\Delta(\mathbf{r})$ is the superconducting order parameter, E is the quasiparticle energy, $(\dots)_N$ denotes a matrix in Nambu space,

$$H_0(\mathbf{r})=-\frac{\hbar^2\nabla^2}{2m}-\frac{\hbar^2k_F^2}{2m}, \tag{4}$$

and m is the electron mass. For brevity, unit matrices in spin and Nambu spaces are omitted in Eq. (2). The electric potential consists of two components:

$$U(\mathbf{r})=V(\mathbf{r})+\sum_l U_l(\mathbf{r}), \tag{5}$$

where $V(\mathbf{r})$ is the "external" potential: in our case, $V(\mathbf{r})=0$ in the superconductor and $V(\mathbf{r})=\infty$ in vacuum. Each term $U_l(\mathbf{r})$ represents the electric potential of the lth magnetic impurity. The exchange field consists of the exchange fields $\mathbf{J}_l$ of all impurities:

$$\mathbf{J}(\mathbf{r})=\sum_l \mathbf{J}_l(\mathbf{r}). \tag{6}$$

In the following, we will consider the magnetic atoms as point impurities. Formally, this means that the potentials $U_l(\mathbf{r})$ and $\mathbf{J}_l(\mathbf{r})$ of the lth atom are localized in a region with a size much smaller than k_F^{-1} in the vicinity of the point $\mathbf{r}_l$. Then, the atoms are predominantly isotropic scatterers, i.e., effective sources of spherical waves. Let us assume that $\mathbf{J}_l(\mathbf{r})=J_l(\mathbf{r})\mathbf{n}_l$, where $\mathbf{n}_l$ are unit vectors. Then, electrons with spins directed along $\mathbf{n}_l$ are scattered with a scattering phase $\alpha_\uparrow$ and without spin rotation. The same holds for electrons with spins directed against $\mathbf{n}_l$, but they generally have a different scattering phase—$\alpha_\downarrow$.[1] In the case of a nonmagnetic impurity, both scattering phases coincide. Generally, the scattering phases are energy-dependent, however, in the narrow energy range $-\Delta_0<E<\Delta_0$ that we will consider, they are approximately constant.

[1]When the vector field $\mathbf{J}_l(\mathbf{r})$ has a noncollinear structure and even is nonlocal, within the isotropic scattering approximation still a vector $\mathbf{n}_l$ can be found such that electrons with spins directed along $\mathbf{n}_l$ or against it are scattered without spin rotation. This follows from the conservation of probability in scattering processes.

Let us put the origin at the position of one of the atoms. Then we can number the impurities in such a way that $\mathbf{r}_l=l\mathbf{a}$, where $\mathbf{a}=(0,0,a)$. Correspondingly, the vectors $\mathbf{n}_l$ are given by

$$\mathbf{n}_l=\mathbf{n}_0\cos(l\varphi)-\mathbf{n}_0\times\mathbf{n}\sin(l\varphi)+(1-\cos(l\varphi))(\mathbf{n}_0\mathbf{n})\mathbf{n}, \tag{7}$$

where $\mathbf{n}$ is the vector relative to which the impurity spins rotate, $\mathbf{n}_0$ is $\mathbf{n}_l$ with $l=0$, φ is the relative rotation angle of the spins (and of the vectors $\mathbf{n}_l$) of two adjacent impurities, $\mathbf{n}_0\mathbf{n}=\cos\chi$, and χ is the tilt angle of the spin helix—see inset in Fig. 1.

The ideology behind the method of solving Eq. (2) is based on the observation that the terms containing $U_l(\mathbf{r})$ and $\mathbf{J}_l(\mathbf{r})$ can be formally considered as point sources in the BdG equations. Since the solutions of BdG equations with point sources are the real-time Green functions, we can write $\Psi(\mathbf{r})$ in the form

$$\Psi=\check{\tau}_z\sum_l \check{G}_E(\mathbf{r},\mathbf{r}_l)\tilde{\Psi}_l, \tag{8}$$

$$\tilde{\Psi}_l=\exp(-i\varphi\check{\boldsymbol{\sigma}}\mathbf{n}l/2)\Psi_l, \tag{9}$$

where Ψ_l are some constant vectors, $\check{G}_E(\mathbf{r},\mathbf{r}')$ is the retarded Green function of the clean Josephson junction, and the exponential factor in Eq. (9) is added to simplify subsequent equations. The Green function satisfies the Gor'kov equation [53]

$$\left[H_0(\mathbf{r})+V(\mathbf{r})-\check{\tau}_z(E+i\eta^+)+\begin{pmatrix}0 & -\Delta(\mathbf{r})\\ \Delta^*(\mathbf{r}) & 0\end{pmatrix}_N\right]\check{G}_E(\mathbf{r},\mathbf{r}')=\delta(\mathbf{r}-\mathbf{r}'), \tag{10}$$

where η^+ is an infinitely small positive quantity. It can be seen that the function given by Eq. (8) satisfies Eq. (2) everywhere, except the close vicinity of impurities, where $U_l(\mathbf{r})\neq 0$ or $\mathbf{J}_l(\mathbf{r})\neq 0$.

Since the BdG Hamiltonian without magnetic atoms contains no exchange terms, the matrix $\check{G}_E(\mathbf{r},\mathbf{r}')$ is diagonal with respect to spin indices and has the form

$$\check{G}_E(\mathbf{r},\mathbf{r}')=\begin{pmatrix}G_E(\mathbf{r},\mathbf{r}') & F_E(\mathbf{r},\mathbf{r}')\\ -F_E^\dagger(\mathbf{r},\mathbf{r}') & \bar{G}_E(\mathbf{r},\mathbf{r}')\end{pmatrix}_N. \tag{11}$$

The components of the matrix $\check{G}_E(\mathbf{r},\mathbf{r}')$ satisfy the following relations:

$$\bar{G}_E(\mathbf{r},\mathbf{r}')=G^*_{-E}(\mathbf{r},\mathbf{r}'),\quad F_E(\mathbf{r},\mathbf{r}')=F^{\dagger *}_{-E}(\mathbf{r},\mathbf{r}'). \tag{12}$$

We will consider only energies lying within a spectral gap of the clean superconductor, so the term $i\eta^+$ can be dropped in Eq. (10). Then, the following additional symmetries arise:

$$G_E(\mathbf{r},\mathbf{r}')=G^*_E(\mathbf{r}',\mathbf{r}),\quad F^\dagger_E(\mathbf{r},\mathbf{r}')=F^\dagger_{-E}(\mathbf{r}',\mathbf{r}). \tag{13}$$

By considering the behavior of the wave function $\Psi(\mathbf{r})$ in the vicinity of the impurities it can be demonstrated that the vectors Ψ_l satisfy the following equations (see Appendix A

for a derivation):

$$\frac{mk_F}{2\pi\hbar^2}\left(\frac{1+\check{\tau}_z\mathbf{n}_0\check{\boldsymbol{\sigma}}}{2}\cot\alpha_\uparrow+\frac{1-\check{\tau}_z\mathbf{n}_0\check{\boldsymbol{\sigma}}}{2}\cot\alpha_\downarrow\right)\Psi_l-\check{G}_{ER}(0,0)\Psi_l-\sum_{n\neq l}\check{G}_E(\mathbf{a}(l-n),0)\exp(i\varphi\check{\boldsymbol{\sigma}}\mathbf{n}(l-n)/2)\Psi_n=0, \quad (14)$$

where

$$\check{G}_{ER}(\mathbf{r},\mathbf{r}')=\check{G}_E(\mathbf{r},\mathbf{r}')-\frac{m}{2\pi\hbar^2|\mathbf{r}-\mathbf{r}'|} \quad (15)$$

is finite for $\mathbf{r}=\mathbf{r}'$. Equation (14) represents a generalization of the linear system derived in Ref. [18] to the case of nonuniform superconductivity and independent scattering phases $\alpha_\uparrow$ and $\alpha_\downarrow$.

III. SHIBA BANDS

In this section, we will study impurity states localized at an infinite chain, so that $l=-\infty\cdots+\infty$. Due to translational invariance, the solutions of Eq. (14) should be sought in the form

$$\Psi_l=e^{iql}\Psi_0, \quad (16)$$

where q is a dimensionless quasi-momentum. Then, the energy versus q dependence can be determined from the equation

$$\det\left\{\frac{mk_F}{2\pi\hbar^2}\left(\frac{1+\check{\tau}_z\mathbf{n}_0\check{\boldsymbol{\sigma}}}{2}\cot\alpha_\uparrow+\frac{1-\check{\tau}_z\mathbf{n}_0\check{\boldsymbol{\sigma}}}{2}\cot\alpha_\downarrow\right)-\check{G}_{ER}(0,0)-\sum_{n\neq0}\check{G}_E(-n\mathbf{a},0)e^{iqn-in\varphi\check{\boldsymbol{\sigma}}\mathbf{n}/2}\right\}=0. \quad (17)$$

For our particular geometry and for $la\ll h,\xi$ the Green functions have been calculated in Ref. [50] (there, the Green function in the absence of impurities was denoted as $\hat{G}_E^{(0)}$):

$$\frac{2\pi\hbar^2}{mk_F}\check{G}_E(l\mathbf{a},0)=\frac{\cos(k_Fal)}{k_Fa|l|}+\frac{\sin(k_Fal)}{2k_Fal}\begin{pmatrix}\cot\left(\gamma+\frac{\theta}{2}\right)+\cot\left(\gamma-\frac{\theta}{2}\right) & \sin^{-1}\left(\gamma+\frac{\theta}{2}\right)+\sin^{-1}\left(\gamma-\frac{\theta}{2}\right)\\ -\sin^{-1}\left(\gamma+\frac{\theta}{2}\right)-\sin^{-1}\left(\gamma-\frac{\theta}{2}\right) & -\cot\left(\gamma+\frac{\theta}{2}\right)-\cot\left(\gamma-\frac{\theta}{2}\right)\end{pmatrix}_N, \quad (18)$$

$$\frac{2\pi\hbar^2}{mk_F}\check{G}_{ER}(0,0)=\frac{1}{2}\begin{pmatrix}\cot\left(\gamma+\frac{\theta}{2}\right)+\cot\left(\gamma-\frac{\theta}{2}\right) & \sin^{-1}\left(\gamma+\frac{\theta}{2}\right)+\sin^{-1}\left(\gamma-\frac{\theta}{2}\right)\\ -\sin^{-1}\left(\gamma+\frac{\theta}{2}\right)-\sin^{-1}\left(\gamma-\frac{\theta}{2}\right) & -\cot\left(\gamma+\frac{\theta}{2}\right)-\cot\left(\gamma-\frac{\theta}{2}\right)\end{pmatrix}_N, \quad (19)$$

where $\gamma=\arccos(E/\Delta_0)$. The quasiclassical approximation was used to derive Eqs. (18) and (19), which is applicable when $k_F\xi\gg1$. For $la\gtrsim h$, one may expect that the Green functions will depend on the shape of the constriction.

Formally putting $a=\infty$, we can determine the energies of YSR states modified by the Josephson phase difference [50]:

$$E=\pm\Delta_0\cos\left(\Theta\pm\frac{\alpha_\uparrow-\alpha_\downarrow}{2}\right), \quad (20)$$

where

$$\Theta=\arcsin\sqrt{\cos\alpha_\uparrow\cos\alpha_\downarrow\sin^2\frac{\theta}{2}+\sin^2\left(\frac{\alpha_\uparrow-\alpha_\downarrow}{2}\right)}. \quad (21)$$

For $\theta=0$, we obtain a pair of ordinary YSR states. However, when a phase bias is applied ($\theta\neq0$), two additional impurity states appear. Then, when the YSR states hybridize, we should expect four bands to form.

Next, one can prove that there are two YSR states at the Fermi level ($E=0$), if

$$\cos\frac{\theta}{2}=\sqrt{-\tan\alpha_\uparrow\tan\alpha_\downarrow}. \quad (22)$$

Thus we can obtain a zero-energy YSR state by applying a phase bias when $\sqrt{-\tan\alpha_\uparrow\tan\alpha_\downarrow}\leqslant1$.

For a finite distance a, the determinant in Eq. (17) is calculated and analyzed in Appendix B. It is shown that for $\theta\neq0$ and $a>\lambda_F/2$, where $\lambda_F=2\pi/k_F$ is the Fermi wavelength, the spectrum of the impurity states consists of four $E(q)$ branches, two of which merge with the gap edge when $\theta=0$. When $a<\lambda_F/2$, for some values of q there may be less than four branches of impurity states—see discussion in Appendix B.

Some spectra of impurity states are shown in Fig. 2. One can see that the spectral branches exhibit singular behavior. This is connected with the slow $\propto|n|^{-1}$ decay of the terms in the series in Eq. (17), which results in logarithmic singularities of this series for certain values of q. As it was said above, for sufficiently large l one should expect a faster than $\propto|l|^{-1}$ decay (presumably, exponential) of the Green function, given by Eq. (18). This will result in better convergence of the series in Eq. (17), so that the spectral branches $E(q)$ may become analytical.

Apart from the impurity states, the subgap spectrum contains degenerate Andreev states that do not interact with the impurities (not shown in Fig. 2). These states are essentially the same as in a clean junction and have energies $E=\pm\Delta_0\cos(\theta/2)$. Depending on the parameters of our system, the quasiparticle spectrum may be gapped or gapless. It is found (see Appendix B) that for $\chi=\pi/2$ and for arbitrarily chosen values of all other parameters the spectrum almost certainly has a gap. This indicates that $\chi=\pi/2$ is most favorable for the observation of MZMs at the ends of the impurity chain (similarly to the case of a helical chain in a

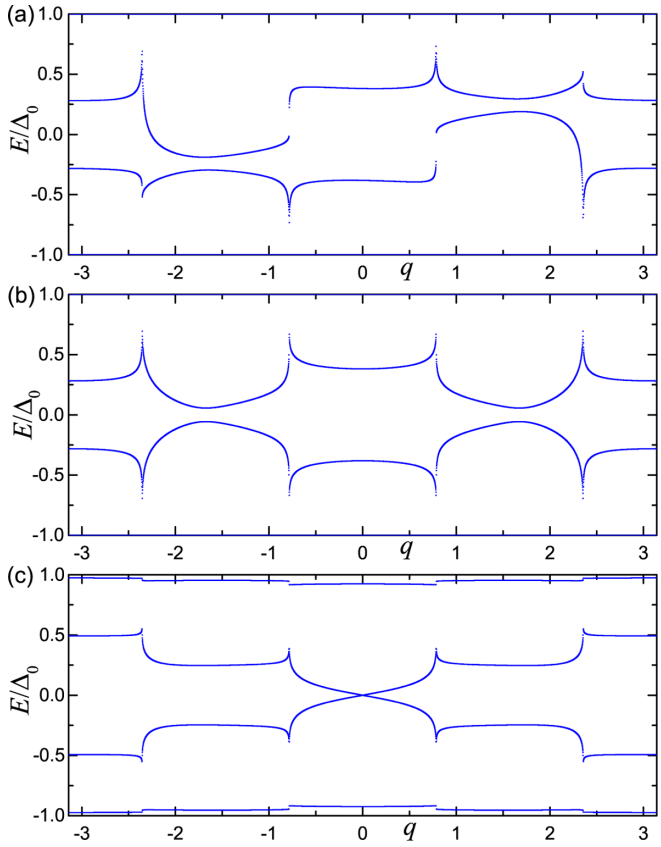

FIG. 2. Spectra of impurity-induced quasiparticle states in the presence of an infinite chain of magnetic point impurities. In all graphs $k_F a = 3\pi/2$, $\varphi = \pi/2$, $\alpha_\uparrow = -\alpha_\downarrow = \pi/4$. The parameters θ and χ are different for (a)–(c). (a)$\chi = \pi/4$, $\theta = 0$—example of a gapless spectrum. (b)$\chi = \pi/2$, $\theta = 0$—a gapped spectrum in a topologically nontrivial phase. (c): $\chi = \pi/2$, $\theta = 1.677$—spectrum at a transition from a topologically nontrivial to a trivial state with a gap closure at $q = 0$. In graphs (a) and (b), corresponding to $\theta = 0$, two of the four YSR bands have merged with the gap edge.

uniform superconductor [14]), the existence of which requires a gapped spectrum.

IV. MAJORANA EDGE MODES

A. Phase diagram

Now we will determine the conditions under which the system is in a topologically nontrivial state, such that MZMs appear at the ends of a finite impurity chain. In the case of discrete translationally invariant BdG Hamiltonians, the general conditions for this have been derived by Kitaev [3]. His results are not directly applicable to our system, because Eq. (14) does not have the form of an eigenvalue problem for some Hamiltonian. However, in the limit $|E| \ll \Delta_0 \cos(\theta/2)$, by linearizing the Green functions with respect to E [using Eqs. (18) and (19)], we can cast Eq. (14) in the form

$$(\check{\mathcal{H}} - E\check{C})\bar{\Psi} = 0, \tag{23}$$

where $\check{\mathcal{H}}$ is a Hermitian operator acting on a vector $\bar{\Psi}$ composed of vectors Ψ_l with all valid numbers l, and $\check{C}$ is a positive definite operator. If we are only interested in MZMs, we may consider a semi-infinite chain, so that $l = 0, 1, 2\ldots$, and put $E = 0$ in Eq. (23). Then, if the number of solutions of the equation $\check{\mathcal{H}}\bar{\Psi} = 0$ is odd, there is a robust Majorana mode at the end of the chain, and there is no robust Majorana mode otherwise (multiple MZMs are not robust with respect to perturbations). It can be demonstrated that the operator $\check{\mathcal{H}}$ is formally equivalent to a discrete BdG Hamiltonian, and hence we can use Kitaev's results to calculate the $\mathbb{Z}_2$ index of the Altland-Zirnbauer class D [54–56]—the Majorana number $\mathcal{M}$. For some values of the parameters the system may belong to a different symmetry class than D (e.g., BDI), however, the additional symmetries are not robust with respect to small perturbations of $\Delta(\mathbf{r})$, $V(\mathbf{r})$, and $\mathbf{J}(\mathbf{r})$, and for this reason we will not consider the corresponding topological indices.

It is proven in Appendix C that the Majorana number for our system is given by

$$\mathcal{M} = \mathrm{sgn}\Big[L\Big(\frac{\varphi}{2}\Big)L\Big(\frac{\varphi}{2}+\pi\Big)\Big], \tag{24}$$

where

$$L(\alpha) = \tilde{l}^2(\alpha) + \frac{2}{1+\cos\theta}\tilde{h}^2(\alpha) - \Big(\frac{\cot\alpha_\uparrow - \cot\alpha_\downarrow}{2}\Big)^2, \tag{25}$$

and the functions $\tilde{h}(\alpha)$ and $\tilde{l}(\alpha)$ are given by Eqs. (B2) and (B3), respectively. The system is in a topologically trivial state when $\mathcal{M} = 1$, and it is in a topologically nontrivial one when $\mathcal{M} = -1$. For the existence of MZMs, $\mathcal{M} = -1$ is required, and in addition the bulk spectrum of the atomic chain must be gapped. It can be seen that Eqs. (24) and (25) do not depend on χ, which may give the impression that a helical spin structure is not necessary for the observation of MZMs. However, it turns out that for a ferromagnetic spin order ($\chi = 0$) the bulk spectrum of the chain is gapped only in the topologically trivial state, as demonstrated in Appendix B. On the other hand, for an antiferromagnetic order ($\varphi = \pi$), $\mathcal{M} = -1$ is impossible, because $L(\pi/2) = L(3\pi/2)$. This means that a helical spin structure is crucial for the observation of MZMs.

In the dilute limit—$k_F a \gg 1$—we have $\tilde{l}(\alpha) \approx -(\cot\alpha_\uparrow + \cot\alpha_\downarrow)/2$ (except for some special combinations of parameters) and $\tilde{h}(\alpha) \approx 1$. Then, $L(\alpha)$ is approximately constant, and a topologically nontrivial state may exist only for $L(\alpha) \approx 0$, when Eq. (22) is approximately satisfied. This restriction can be explained as follows. To obtain a topologically nontrivial state, roughly speaking, two YSR bands have to overlap at $q = 0$ or $q = \pi$. In the dilute limit, the YSR bands become narrow, and an overlap is possible only when the energies of isolated YSR states are close to zero, i.e., Eq. (22) is satisfied. This consideration also implies that the size of the topological gap is roughly bounded from above by the width of the YSR bands, which is much smaller than Δ_0 in the dilute limit. For a more dense atom chain, the topological gap may be of the order of Δ_0, which is more favorable for manipulations with MZMs.

In the dense limit, which is characterized by the inequality $k_F a \ll \pi$, it turns out that $\tilde{h}(\alpha)$ [Eq. (B2)] vanishes for almost all α. As a result, the Majorana number does not depend on θ (except for some very specific values of φ). This means that the topological state of the atom chain can not be manipulated by applying a phase bias. Thus, in the context of the constriction geometry, the most interesting case is $k_F a \sim \pi$. In the

present paper, in numerical calculations the value $k_F a = 1.5\pi$ is used.

Now we will discuss the dependence of the topological state on the phase θ. Let us consider θ in the range $[0, \pi]$—the spectrum is invariant under the replacement of θ by $-\theta$. Depending on the parameters a, χ and φ, the quasiparticle spectrum is affected by variations of θ in different ways. First, assume that for $\theta = 0$ the system is in a topologically nontrivial state. We may note that $L(\alpha)$ is a monotonically increasing function of θ (provided that $a > \lambda_F/2$, so that $\tilde{h}(\alpha) \neq 0$). Then, as θ is increased, both $L(\varphi/2)$ and $L(\varphi/2 + \pi)$ become positive, which means that the system switches to a topologically trivial state. At intermediate values of θ, a gapless state exists, such that two of the $E(q)$ branches touch the zero-energy level either at $q = 0$ or at $q = \pi$. A typical spectrum of an infinite chain at the topological phase transition point is shown in Fig. 2(c), where the spectral gap closes at $q = 0$. Next, consider the case when the system is in a topologically trivial state when $\theta = 0$. If both $L(\varphi/2)$ and $L(\varphi/2 + \pi)$ are positive for $\theta = 0$, then no topological phase transitions happen as θ is increased. On the other hand, if both $L(\varphi/2)$ and $L(\varphi/2 + \pi)$ are negative for $\theta = 0$, two topological phase transitions may take place as θ is increased from 0 to π.

In Fig. 3, two characteristic phase diagrams of the system are shown. In the gapped phases, the color shows the gap in the bulk spectrum of the chain—this quantity is the topological gap in the regime where isolated Majorana fermions exist. It should be borne in mind that the gap is limited from above by $\Delta_0 \cos(\theta/2)$, which is the energy of Andreev states that do not interact with the impurities. Hence, at $\theta = \pi$ the spectrum is gapless. Figure 3(a) corresponds to the case where the system is in a topologically nontrivial state even when $\theta = 0$. Still, the Josephson phase difference can be used to enhance the topological gap: the gap is the largest for $\theta \approx 1.29$ when $\chi = \pi/2$.

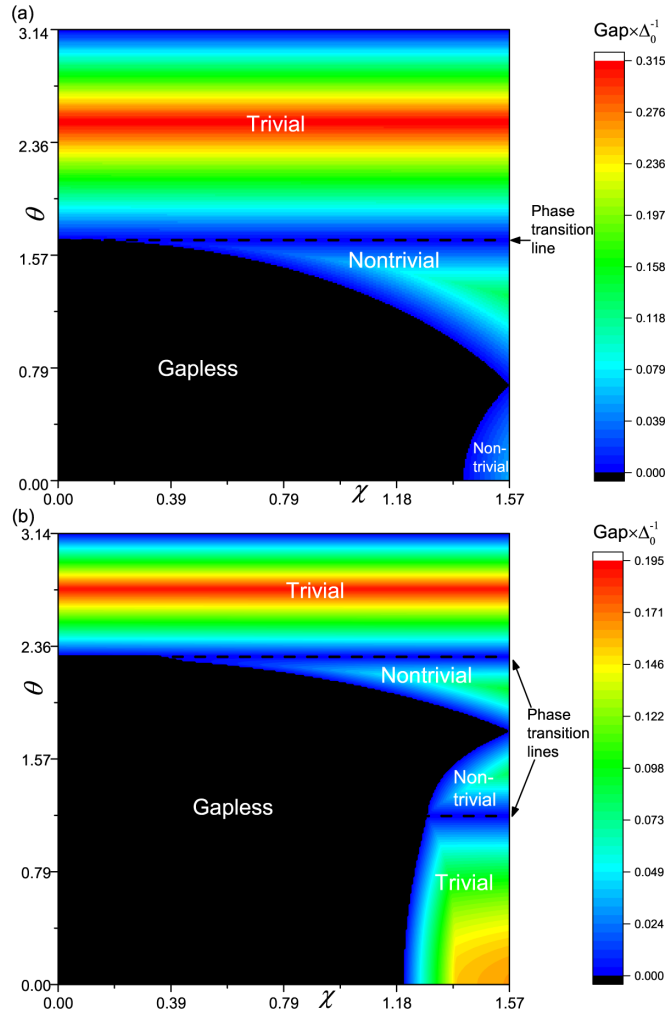

FIG. 3. The spectral gap and the phase diagram of the impurity chain in the $\chi - \theta$ plane. The parameters used are (a) $k_F a = 3\pi/2$, $\alpha_\uparrow = -\alpha_\downarrow = \pi/4$, $\varphi = \pi/2$ and (b) $k_F a = 3\pi/2$, $\alpha_\uparrow = \pi/4$, $\alpha_\downarrow = -\pi/8$, $\varphi = \pi/3$.

B. Wave functions of Majorana edge states

In this section, we will briefly discuss the structure of the low-energy $[E \ll \Delta_0 \cos(\theta/2)]$ quasiparticle excitations localized at a finite impurity chain, and, in particular, the structure of Majorana modes. The energies and wave functions of low-energy excitations are determined from Eq. (23), which constitutes a generalized eigenvalue problem that can be solved using standard numerical routines. The numerical solution of Eq. (23) has been performed for a chain with 400 atoms ($l = 1, \ldots, 400$). The obtained quantities $\|\Psi_l\|^2$ with appropriate normalization can be roughly interpreted as the probabilities to find a quasiparticle in the vicinity of the lth atom, where $\|\ldots\|$ denotes the ℓ^2-norm of a vector.[2] Some characteristic spatial profiles of the four impurity-induces states with lowest energies are shown in Fig. 4. The Majorana edge modes in the topologically nontrivial state can be clearly seen, and in the topologically trivial state, no low-energy edge modes can be observed.

It should be noted that the coefficients in Eq. (14) decay with $|l - n|$ in a power-law manner. This indicates that the wave functions of edge states might exhibit a nonexponential decay with increasing distance from the edge of the chain [57–59]. For a helical atom chain in a bulk superconductor, this issue was studied by Pientka *et al.* [14,51], who developed a two-band approximation for Eq. (14) in the dilute limit—$k_F a \gg 1$—and for $\alpha_\uparrow = -\alpha_\downarrow$. In this limit, for low energies, Eq. (14) can be reduced to a system of ordinary discrete BdG equations:

$$\sum_m \begin{pmatrix} t(l-m) & \Delta(l-m) \\ \Delta^*(m-l) & -t(m-l) \end{pmatrix} \begin{pmatrix} u_m \\ v_m \end{pmatrix} = \epsilon \begin{pmatrix} u_l \\ v_l \end{pmatrix}, \quad (26)$$

where l and m are indices numbering the impurities, u_m and v_m are the expansion coefficients of the quasiparticle wave function in terms of the wave functions of YSR states

[2]Strictly speaking, this is not correct: the vectors Ψ_l influence the probability to find a quasiparticle not only close to the lth impurity, but also far from it due to the slow decay of the Green function $\check{G}_E(\mathbf{r}, \mathbf{r}')$ with the distance between $\mathbf{r}$ and $\mathbf{r}'$. Still, the quantities $||\Psi_l||^2$ allow to clearly visualize the difference between MZMs and the bulk modes of the chain.

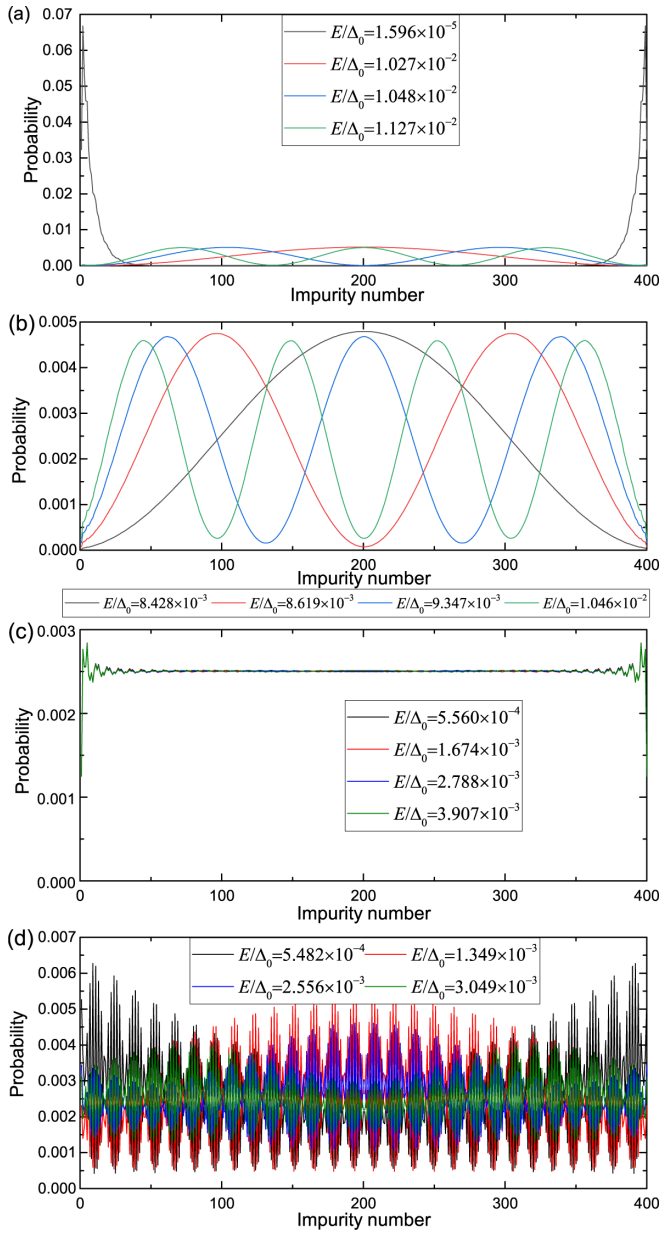

FIG. 4. Profiles of the four quasiparticle excitations with the lowest energies in the presence of a chain with 400 impurities: the probability to find a quasiparticle in the vicinity of each impurity is plotted. The energies of quasiparticles are shown in each panel. The following parameters are used: $k_F a = 1.5\pi$, $\chi = \pi/2$, $\alpha_\uparrow = -\alpha_\downarrow = \pi/4$. (a) $\theta = 1.65$: topologically nontrivial state. The Majorana edge state can be clearly seen. (b) $\theta = 1.7$: topologically trivial state. (c) $\theta = 1.67727$: gapless state at the topological phase transition. (d) $\theta = 0.67$: topologically nontrivial state close to the gapless phase.

localized at the mth atom (there are two such states with energies $\pm\Delta_0 \cos(2\alpha_\uparrow)$), $t(l)$ and $\Delta(l)$ are hopping and pairing amplitudes, respectively [see Eqs. (D1) and (D2) for explicit formulas], and $\epsilon = E/\Delta_0$. By analyzing the numerical solutions of Eq. (26), it was found that the envelope for the amplitudes Ψ_l for large l in a very long chain with $l = 0, 1, 2\ldots$ is proportional to $1/(l \ln^2 l)$ [14]. This was then confirmed analytically for a planar helix ($\chi = \pi/2$) and for $\varphi/2 \approx k_F a$ [51].

In Appendix D, using Eq. (14), we generalize the two-band approximation of Pientka *et al.* to the case of a short Josephson junctions and for arbitrary phases $\alpha_\uparrow$ and $\alpha_\downarrow$ (not limited to $\alpha_\uparrow = -\alpha_\downarrow$). The generalization amounts to a modification of the coefficients $t(l)$ and $\Delta(l)$—see Eqs. (D4) and (D5). We find that in the topologically nontrivial state Eq. (26) admits an exact analytical solution for a MZM ($\epsilon = 0$) on a semi-infinite atom chain in the case of a planar spin helix: $\chi = \pi/2$. The explicit solution is somewhat cumbersome (see Appendix D), however, its asymptotic behavior for large l is relatively simple. We find that the amplitudes Ψ_l are approximately given by

$$\Psi_l \approx \Psi^{(1)}\left[\frac{1}{l(\ln l)^{\mu_1}}\cos\left(l\left(k_F a \pm \frac{\varphi}{2}\right)+\beta_1\right)\right.$$
$$\left.+\frac{C}{l(\ln l)^{\mu_2}}\cos\left(l\left(k_F a \mp \frac{\varphi}{2}\right)+\beta_2\right)\right], \qquad (27)$$

where $\Psi^{(1)}$ is a vector and C, β_1, β_2 are numbers that do not depend on l, and

$$\mu_{1,2} = \frac{3}{2} \pm \frac{1}{2\cos\frac{\theta}{2}}. \qquad (28)$$

The $\pm$ and $\mp$ symbols in Eq. (27) should be replaced by either a plus or a minus depending on the sign of a winding number [Eq. (D18)]. For $\theta = 0$, which formally corresponds to a uniform superconductor, it turns out that $C = 0$. Additionally, in this case $\mu_1 = 2$, and we simply obtain an extension of the results from Ref. [51] to a wider range of the parameters φ, $\alpha_\uparrow$ and $\alpha_\downarrow$. However, $C \neq 0$ for $\theta \neq 0$, and then for sufficiently large l the term in the second line of Eq. (27) dominates. Thus, in the presence of a Josephson phase bias and for sufficiently large distances from the edge of the atom chain one should put $\mu = \mu_2$ in Eq. (1).

To finish the discussion of MZM wave functions, we note that Eq. (18) for the Green functions is applicable for $|l|a \ll h$. For $|l|a \gtrsim \xi$ we may expect that the Green functions will exhibit exponential decay with increasing $|l|$ due to the presence of the superconducting gap (details of the behavior of the Green functions depend on the shape of the constriction). Thus Eq. (27) describes intermediate asymptotic behavior of a MZM wave function for $1 \ll l \ll \xi/a$. For $l \gg \xi/a$, the MZM will be exponentially localized.

V. POSSIBLE EXPERIMENTAL IMPLEMENTATIONS

The physical model that we have considered illustrates a key concept: if we can manipulate the energies of YSR states via a Josephson phase, then we can tune the topological state of the helical atom chain. In this context, to construct a system with a tunable topological state, we need the following three components: (i) a short, but relatively wide Josephson junction with a gapped quasiparticle spectrum and transparent transport channels, (ii) a helical atom chain, and (iii) low disorder in the vicinity of the chain. A short junction is preferable to a long one because of larger phase gradients and a larger spectral gap, which can be of the order of the bulk gap. In a junction with low transparency, the energies of YSR states

weakly depend on the Josephson phase θ, and hence we need highly transparent channels. Finally, nonmagnetic disorder affects the energies of YSR states as well as hopping amplitudes between magnetic atoms, making these quantities random. For this reason, a clean system is preferable.

A possible real physical system that is relatively close to the studied idealized model would be a Re-based junction with an iron atom chain on top of it. A Fe spin helix forms spontaneously in the presence of Re [31]. Moreover, in Re the product of the superconducting gap and of the normal density of states per atom is very small [60], so that the quasiclassical approximation is applicable.

An alternative structure satisfying the requirements (i)–(iii) could be a superconductor-2D electron gas (2DEG)-superconductor junction. To minimize effects of disorder, it would be optimal to use an epitaxial structure with a high-mobility 2DEG, like in Refs. [61,62]. The atomic chain can be placed on the semiconductor or on a superconducting electrode close to the junction. The geometries of such structures are clearly very different from the one shown in Fig. 1, so that the quantitative results from Secs. III and IV are not directly applicable.

For any experimental prototype, the key point is the dependence of the energies of isolated YSR on the phase difference θ. Therefore it is reasonable to detect this dependence (using, e.g., scanning tunneling microscopy) before studying the properties of atomic chains.

VI. CONCLUSION

To sum up, we have studied the subgap quasiparticle spectrum and topological phase diagram of a helical magnetic atom chain located inside a weak link of the constriction type. We found that an infinite chain supports four Shiba bands if the Josephson phase difference θ is nonzero (otherwise, there are two bands). For a nonplanar spin helix, a gapless phase exists, and for a planar helix the quasiparticle spectrum is almost certainly gapped, which makes the planar configuration most favorable for the observation of MZM localized at the ends of the atom chain.

The Majorana number for our system has been calculated, and it has been found that it does not depend on the tilt angle χ of the spin helix. It has been demonstrated that the Josephson phase difference can be used to switch the system between the topologically trivial and nontrivial states even if the YSR states induced by isolated magnetic atoms are initially (for $\theta = 0$) not deep. By applying a phase difference θ, one can also enhance the topological gap. However, for collinear spin structures the system is always in a topologically trivial or gapless state.

The structure of Majorana edge modes has been analyzed. The approximate two-band system of discrete BdG equations derived by Pientka *et al.* [14] has been generalized to include a Josephson phase difference. For a planar spin helix, an exact analytical solution for the wave function of a MZM localized at the end of a semi-infinite chain has been obtained. For $\theta = 0$ this solution constitutes an extension of the solution obtained by Pientka *et al.* for a bulk superconductor [51] to the whole topological phase: the wave function of a MZM falls off with distance from the end of the chain in accordance with Eq. (1) with $\mu = 2$. However, when a Josephson phase bias is applied, one obtains an asymptotic behavior of the MZM wave function with the exponent μ depending on θ: in particular, for sufficiently large distances s we have $\mu = \mu_2$ [see Eq. (28)].

ACKNOWLEDGMENTS

I am grateful to I. A. Shereshevskii and M. S. Shustin for stimulating discussions and to A. S. Mel'nikov for useful remarks on the manuscript. The work has been supported by Russian Science Foundation Grant No. 21-12-00409.

APPENDIX A: BOGOLIUBOV-DE GENNES EQUATIONS WITH POINT IMPURITIES

In this Appendix, it will be demonstrated how to properly take into account point impurities in the BdG equations in the case of an inhomogeneous superconductor, and Eq. (14) will be derived.

For simplicity, we put $\mathbf{J}_l(\mathbf{r}) = J_l(\mathbf{r})\mathbf{n}_l$. The considerations given below can be generalized for the case when the vectors $\mathbf{J}_l(\mathbf{r})$ for different $\mathbf{r}$ are not collinear.

Let us introduce the following vectors:

$$\Phi_{l\pm}(\mathbf{r}) = \frac{1 \pm \check{\tau}_z \mathbf{n}_l \check{\boldsymbol{\sigma}}}{2} \Psi(\mathbf{r}). \tag{A1}$$

Since $(1 \pm \check{\tau}_z \mathbf{n}_l \check{\boldsymbol{\sigma}})/2$ are projection matrices, the following relations hold:

$$\frac{1 \pm \check{\tau}_z \mathbf{n}_l \check{\boldsymbol{\sigma}}}{2} \Phi_{l\pm}(\mathbf{r}) = \Phi_{l\pm}(\mathbf{r}), \quad \frac{1 \mp \check{\tau}_z \mathbf{n}_l \check{\boldsymbol{\sigma}}}{2} \Phi_{l\pm}(\mathbf{r}) = 0. \tag{A2}$$

If we multiply Eq. (2) by $(\check{\tau}_z \pm \mathbf{n}_l \check{\boldsymbol{\sigma}})/2$, we obtain in the vicinity of the lth impurity

$$[H_0(\mathbf{r}) + U_l(\mathbf{r}) \pm J_l(\mathbf{r})]\Phi_{l\pm}(\mathbf{r}) = 0. \tag{A3}$$

Here, we neglected the terms containing $\Delta(\mathbf{r})$ and E, which have a negligibly small effect on the wave function on spatial scales that are much smaller than ξ. It can be seen that in the vicinity of the impurity $\Phi_{l\pm}(\mathbf{r})$ satisfies an ordinary Schrödinger equation. Then, it follows from general scattering theory that in the vicinity of the lth impurity $\Phi_{l\pm}(\mathbf{r})$ can be written in the form (see Appendix B in Ref. [50] for a detailed derivation)

$$\Phi_{l\pm}(\mathbf{r}) \approx A_{l\pm} + \frac{A_{l\pm} \tan \alpha_{l\pm}}{k_F |\mathbf{r} - \mathbf{r}_l|}, \tag{A4}$$

where $A_{l\pm}$ are constant vectors, and $\alpha_{l\pm}$ are scattering phases corresponding to the potentials $U_l(\mathbf{r}) \pm J_l(\mathbf{r})$. Note that Eq. (A4) is valid for $\mathbf{r}$ lying outside the range of the potentials $U_l(\mathbf{r})$ and $J_l(\mathbf{r})$, and the condition $k_F|\mathbf{r} - \mathbf{r}_l| \ll 1$ should be satisfied. Let us introduce the vector $A_l = A_{l+} + A_{l-}$. It follows from Eq. (A2) that

$$\frac{1 \pm \check{\tau}_z \mathbf{n}_l \check{\boldsymbol{\sigma}}}{2} A_{l\pm} = A_{l\pm}, \quad \frac{1 \mp \check{\tau}_z \mathbf{n}_l \check{\boldsymbol{\sigma}}}{2} A_{l\pm} = 0, \tag{A5}$$

and hence

$$\frac{1 \pm \check{\tau}_z \mathbf{n}_l \check{\boldsymbol{\sigma}}}{2} A_l = A_{l\pm}. \tag{A6}$$

Now we sum Eq. (A4) with the plus and minus subscript and eliminate $A_{l\pm}$ from the equations using Eq. (A6) to obtain

$$\Psi(\mathbf{r}) \approx A_l + \left(\frac{1+\check{\tau}_z \mathbf{n}_l \check{\boldsymbol{\sigma}}}{2}\tan\alpha_{l+} + \frac{1-\check{\tau}_z \mathbf{n}_l \check{\boldsymbol{\sigma}}}{2}\tan\alpha_{l-}\right)\frac{A_l}{k_F|\mathbf{r}-\mathbf{r}_l|}. \tag{A7}$$

On the other hand, to satisfy the BdG equations far from the impurities $\Psi(\mathbf{r})$ should have the form (8). Using Eq. (15), in the vicinity of the lth impurity we find that

$$\Psi(\mathbf{r}) \approx \check{\tau}_z \sum_{n\neq l} \check{G}_E(\mathbf{r}_l, \mathbf{r}_n)\tilde{\Psi}_n + \check{\tau}_z \check{G}_{ER}(\mathbf{r}_l, \mathbf{r}_l)\tilde{\Psi}_l + \frac{m}{2\pi\hbar^2|\mathbf{r}-\mathbf{r}_l|}\check{\tau}_z\tilde{\Psi}_l. \tag{A8}$$

Comparing the right-hand sides of Eqs. (A7) and (A8), we obtain

$$A_l = \check{\tau}_z \sum_{n\neq l} \check{G}_E(\mathbf{r}_l, \mathbf{r}_n)\tilde{\Psi}_n + \check{\tau}_z \check{G}_{ER}(\mathbf{r}_l, \mathbf{r}_l)\tilde{\Psi}_l, \tag{A9}$$

$$\left(\frac{1+\check{\tau}_z \mathbf{n}_l \check{\boldsymbol{\sigma}}}{2}\tan\alpha_{l+} + \frac{1-\check{\tau}_z \mathbf{n}_l \check{\boldsymbol{\sigma}}}{2}\tan\alpha_{l-}\right)\frac{A_l}{k_F} = \frac{m}{2\pi\hbar^2}\check{\tau}_z\tilde{\Psi}_l. \tag{A10}$$

Next, we eliminate A_l from Eq. (A10) using Eq. (A9):

$$\left(\frac{1+\check{\tau}_z \mathbf{n}_l \check{\boldsymbol{\sigma}}}{2}\tan\alpha_{l+} + \frac{1-\check{\tau}_z \mathbf{n}_l \check{\boldsymbol{\sigma}}}{2}\tan\alpha_{l-}\right)\left[\sum_{n\neq l}\check{G}_E(\mathbf{r}_l, \mathbf{r}_n)\tilde{\Psi}_n + \check{G}_{ER}(\mathbf{r}_l, \mathbf{r}_l)\tilde{\Psi}_l\right] = \frac{mk_F}{2\pi\hbar^2}\tilde{\Psi}_l. \tag{A11}$$

Now we invert the matrix in the parentheses and put $\alpha_{l+} = \alpha_\uparrow, \alpha_{l-} = \alpha_\downarrow$:

$$\frac{mk_F}{2\pi\hbar^2}\left(\frac{1+\check{\tau}_z \mathbf{n}_l \check{\boldsymbol{\sigma}}}{2}\cot\alpha_\uparrow + \frac{1-\check{\tau}_z \mathbf{n}_l \check{\boldsymbol{\sigma}}}{2}\cot\alpha_\downarrow\right)\tilde{\Psi}_l - \check{G}_{ER}(\mathbf{r}_l, \mathbf{r}_l)\tilde{\Psi}_l - \sum_{n\neq l}\check{G}_E(\mathbf{r}_l, \mathbf{r}_n)\tilde{\Psi}_n = 0. \tag{A12}$$

Finally, we substitute here Eq. (9). Using translational invariance in the z direction and the relation

$$\mathbf{n}_l\check{\boldsymbol{\sigma}} = \exp(-i\varphi\check{\boldsymbol{\sigma}}\mathbf{n}l/2)\mathbf{n}_0\check{\boldsymbol{\sigma}}\exp(i\varphi\check{\boldsymbol{\sigma}}\mathbf{n}l/2), \tag{A13}$$

we obtain Eq. (14).

APPENDIX B: ANALYSIS OF THE SPECTRUM OF AN INFINITE CHAIN

Here we will analyze the continuous spectrum of quasiparticle states localized in the vicinity of an infinite chain of impurities. For a start, we substitute Eqs. (18) and (19) into Eq. (17). Evaluation of the determinant yields (after cumbersome, but standard calculations)

$$\begin{aligned}
&\left[(\cos\theta-\cos(2\gamma))\tilde{l}^2\left(q-\frac{\varphi}{2}\right)+(1-\cos(2\gamma))\tilde{h}^2\left(q-\frac{\varphi}{2}\right)\right]\left[(\cos\theta-\cos(2\gamma))\tilde{l}^2\left(q+\frac{\varphi}{2}\right)+(1-\cos(2\gamma))\tilde{h}^2\left(q+\frac{\varphi}{2}\right)\right]\\
&-2\left(\frac{\cot\alpha_\uparrow-\cot\alpha_\downarrow}{2}\right)^2\left\{(1-\cos(2\gamma))(2+\cos(2\gamma)+\cos\theta)\tilde{h}\left(q-\frac{\varphi}{2}\right)\tilde{h}\left(q+\frac{\varphi}{2}\right)+(\cos\theta-\cos(2\gamma))^2\right.\\
&\left.\times\tilde{l}\left(q-\frac{\varphi}{2}\right)\tilde{l}\left(q+\frac{\varphi}{2}\right)\right\}+\left(\frac{\cot\alpha_\uparrow-\cot\alpha_\downarrow}{2}\right)^4(\cos\theta-\cos(2\gamma))^2+\cos\chi\,\sin(2\gamma)(\cot\alpha_\uparrow-\cot\alpha_\downarrow)\\
&\times\left\{\tilde{h}\left(q+\frac{\varphi}{2}\right)\left[(\cos\theta-\cos(2\gamma))\left[\tilde{l}^2\left(q-\frac{\varphi}{2}\right)-\left(\frac{\cot\alpha_\uparrow-\cot\alpha_\downarrow}{2}\right)^2\right]+(1-\cos(2\gamma))\tilde{h}^2\left(q-\frac{\varphi}{2}\right)\right]\right.\\
&\left.-\tilde{h}\left(q-\frac{\varphi}{2}\right)\left[(\cos\theta-\cos(2\gamma))\left[\tilde{l}^2\left(q+\frac{\varphi}{2}\right)-\left(\frac{\cot\alpha_\uparrow-\cot\alpha_\downarrow}{2}\right)^2\right]+(1-\cos(2\gamma))\tilde{h}^2\left(q+\frac{\varphi}{2}\right)\right]\right\}\\
&-\cos^2\chi\left(\frac{\cot\alpha_\uparrow-\cot\alpha_\downarrow}{2}\right)^2(\cos\theta-\cos(2\gamma))\left\{(1-\cos(2\gamma))\left[\tilde{h}\left(q-\frac{\varphi}{2}\right)-\tilde{h}\left(q+\frac{\varphi}{2}\right)\right]^2\right.\\
&\left.+(\cos\theta-\cos(2\gamma))\left[\tilde{l}\left(q-\frac{\varphi}{2}\right)-\tilde{l}\left(q+\frac{\varphi}{2}\right)\right]^2\right\}=0,
\end{aligned} \tag{B1}$$

where

$$\tilde{h}(\alpha) = 1+2\sum_{l=1}^{\infty}\frac{\sin(k_F a l)}{k_F a l}\cos(l\alpha) = \frac{\pi}{k_F a}\left(\left\lfloor\frac{\alpha+k_F a}{2\pi}\right\rfloor-\left\lfloor\frac{\alpha-k_F a}{2\pi}\right\rfloor\right), \tag{B2}$$

$$\tilde{l}(\alpha) = 2\sum_{l=1}^{\infty} \frac{\cos(k_F a l)}{k_F a l} \cos(l\alpha) - \frac{\cot\alpha_\uparrow + \cot\alpha_\downarrow}{2}$$
$$= -\frac{1}{2k_F a}[\ln(2 - 2\cos(\alpha + k_F a)) + \ln(2 - 2\cos(\alpha - k_F a))] - \frac{\cot\alpha_\uparrow + \cot\alpha_\downarrow}{2}, \quad \text{(B3)}$$

and $\lfloor\alpha\rfloor$ denotes the floor function. Equation (B1) can be reduced to a quartic equation with respect to e^{2iy}, which can be solved using Ferrari's method [63]. This method has been used to obtain Fig. 2. I was unable to prove that the four roots of the quartic equation always have unit absolute values, however, numerical analysis indicates that this seems to be the case.

It can be seen from Eq. (B2) that when $a < \lambda_F/2$ the function $\tilde{h}(\alpha)$ goes to zero when $k_F a < |\alpha| < \pi$. This means that such range of values of q exists that either $\tilde{h}(q - \varphi/2) = 0$ or $\tilde{h}(q + \varphi/2) = 0$. For such q Eq. (B1) has solutions given by $E = \pm\Delta_0 \cos\theta$. These energies do not depend on any characteristics of impurities and correspond to Andreev states of the clean junction that do not interact with impurities: $\Psi(\mathbf{r}_l) = 0$ for all impurity sites. A characteristic spectrum obtained from Eq. (B1) in this situation is shown in Fig. 5. The above considerations suggest that there can be no more than $8/\lambda_F$ impurity-induced states per unit length of the impurity chain.

Let us derive the conditions for the spectrum given by Eq. (B1) to have a gap. If we put $E = 0$ in Eq. (B1), for $\theta \neq \pi$, we obtain

$$L\left(q + \frac{\varphi}{2}\right)L\left(q - \frac{\varphi}{2}\right) + \sin^2\chi\left(\frac{\cot\alpha_\uparrow - \cot\alpha_\downarrow}{2}\right)^2$$
$$\times \left\{\frac{2}{1+\cos\theta}\left[\tilde{h}\left(q - \frac{\varphi}{2}\right) - \tilde{h}\left(q + \frac{\varphi}{2}\right)\right]^2 + \left[\tilde{l}\left(q - \frac{\varphi}{2}\right)\right.\right.$$
$$\left.\left. - \tilde{l}\left(q + \frac{\varphi}{2}\right)\right]^2\right\} = 0, \quad \text{(B4)}$$

where $L(\alpha)$ is given by Eq. (25). If Eq. (B4) is satisfied for some q, then the spectrum is gapless. We may note that for $q = 0$ the left-hand side of Eq. (B4) is non-negative. Then, assuming that it is a continuous function of q,[3] we find that the necessary and sufficient condition for the spectrum to be gapped is

$$L\left(q + \frac{\varphi}{2}\right)L\left(q - \frac{\varphi}{2}\right) + \sin^2\chi\left(\frac{\cot\alpha_\uparrow - \cot\alpha_\downarrow}{2}\right)^2$$
$$\times \left\{\frac{2}{1+\cos\theta}\left[\tilde{h}\left(q - \frac{\varphi}{2}\right) - \tilde{h}\left(q + \frac{\varphi}{2}\right)\right]^2 + \left[\tilde{l}\left(q - \frac{\varphi}{2}\right)\right.\right.$$
$$\left.\left. - \tilde{l}\left(q + \frac{\varphi}{2}\right)\right]^2\right\} > 0 \quad \text{(B5)}$$

for all q. Now we note that the second term in the left-hand side of Eq. (B5) is a nondecreasing function of χ for $\chi \in [0, \pi/2]$. This means that with increasing χ the range of values of other parameters (e.g., θ, a and others) corresponding to a gapped spectrum becomes broader.

If we put $\chi = 0$ in Eq. (B5), we obtain

$$L\left(q + \frac{\varphi}{2}\right)L\left(q - \frac{\varphi}{2}\right) > 0. \quad \text{(B6)}$$

The function $L(q)$ is positive for some values of q because of the logarithmic singularities in Eq. (B3). Hence, the condition (B6) is equivalent to $L(q) > 0$ for all q. The latter condition is incompatible with the relation $\mathcal{M} = -1$ [see Eq. (24)], which provides a necessary condition for the topologically nontrivial regime. This means that a gapped topologically nontrivial phase does not exist when $\chi = 0$.

Equation (B5) with $\chi = \pi/2$ yields

$$\frac{2}{1+\cos\theta}\left[\tilde{l}\left(q - \frac{\varphi}{2}\right)\tilde{h}\left(q + \frac{\varphi}{2}\right) - \tilde{l}\left(q + \frac{\varphi}{2}\right)\tilde{h}\left(q - \frac{\varphi}{2}\right)\right]^2$$
$$+ \left[\tilde{l}\left(q + \frac{\varphi}{2}\right)\tilde{l}\left(q - \frac{\varphi}{2}\right) - \left(\frac{\cot\alpha_\uparrow - \cot\alpha_\downarrow}{2}\right)^2\right.$$
$$\left. + \frac{2}{1+\cos\theta}\tilde{h}\left(q + \frac{\varphi}{2}\right)\tilde{h}\left(q - \frac{\varphi}{2}\right)\right]^2 > 0. \quad \text{(B7)}$$

The left-hand side of this inequality is a sum of two squares, hence, Eq. (B7) is satisfied when one of the following two inequalities holds:

$$\tilde{l}\left(q - \frac{\varphi}{2}\right)\tilde{h}\left(q + \frac{\varphi}{2}\right) - \tilde{l}\left(q + \frac{\varphi}{2}\right)\tilde{h}\left(q - \frac{\varphi}{2}\right) \neq 0, \quad \text{(B8)}$$

$$\tilde{l}\left(q + \frac{\varphi}{2}\right)\tilde{l}\left(q - \frac{\varphi}{2}\right) - \left(\frac{\cot\alpha_\uparrow - \cot\alpha_\downarrow}{2}\right)^2$$
$$+ \frac{2}{\cos\theta + 1}\tilde{h}\left(q + \frac{\varphi}{2}\right)\tilde{h}\left(q - \frac{\varphi}{2}\right) \neq 0. \quad \text{(B9)}$$

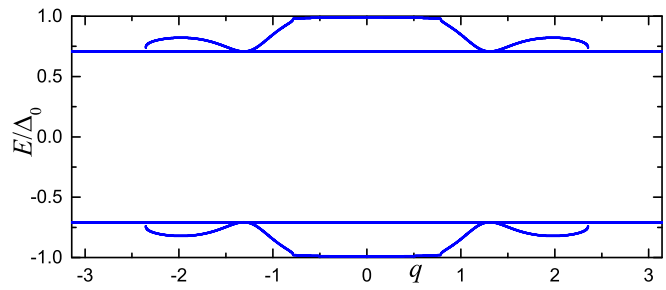

FIG. 5. A typical spectrum (E vs q dependence) obtained from Eq. (B1) when the distance between impurities is smaller than $\lambda_F/2$. The parameters are $k_F a = \chi = \theta = \varphi = \pi/2$ and $\alpha_\uparrow = -\alpha_\downarrow = \pi/4$. The flat bands with $E = \pm\Delta_0 \cos(\theta/2)$ correspond to Andreev states that do not interact with impurities.

[3]Strictly speaking, this is not true in our case, because $\tilde{h}(\alpha)$ and $\tilde{l}(\alpha)$ are discontinuous, which is connected with the slow decay with $|\mathbf{r} - \mathbf{r}'|$ of the Green functions that we use [Eq. (18)]. If we use more realistic expressions for the Green functions in the limit $|\mathbf{r} - \mathbf{r}'| \gtrsim \xi$, the discontinuities disappear.

For arbitrarily chosen parameters of our system, both these inequalities can be simultaneously violated with zero probability. This means that the quasiparticle spectrum is almost certainly gapped when $\chi = \pi/2$.

APPENDIX C: CALCULATION OF THE MAJORANA NUMBER

In this Appendix, we will calculate the Majorana number $\mathcal{M}$ for our impurity chain. To use the results of Kitaev [3], we first need to map Eq. (14) to an eigenvalue problem for a BdG Hamiltonian. For a start, let us put $E = 0$ in Eq. (14):

$$\left(\frac{1+\check{\tau}_z\mathbf{n}_0\check{\boldsymbol{\sigma}}}{2}\cot\alpha_\uparrow + \frac{1-\check{\tau}_z\mathbf{n}_0\check{\boldsymbol{\sigma}}}{2}\cot\alpha_\downarrow\right)\Psi_l - \sum_n \begin{pmatrix} g(l-n) & f^{\dagger *}(l-n) \\ -f^\dagger(l-n) & g^*(l-n)\end{pmatrix}_N e^{i\varphi\check{\boldsymbol{\sigma}}\mathbf{n}(l-n)/2}\Psi_n = 0, \tag{C1}$$

where the following functions of a discrete argument are introduced:

$$g(l) = \begin{cases} \frac{2\pi\hbar^2}{mk_F}G_0(\mathbf{a}l,0) & \text{for} \quad l\neq 0, \\ \frac{2\pi\hbar^2}{mk_F}G_{0R}(0,0) & \text{for} \quad l = 0, \end{cases} \tag{C2}$$

$$f^\dagger(l) = \frac{2\pi\hbar^2}{mk_F}F_0^\dagger(\mathbf{a}l,0). \tag{C3}$$

From Eq. (13), we can derive the relations

$$g(-l) = g^*(l), \qquad f^\dagger(-l) = f^\dagger(l). \tag{C4}$$

Let us direct the z spin quantization axis along the vector $\mathbf{n}$, and let us direct the x axis so that the vector $\mathbf{n}_0$ lies in the xz plane:

$$\mathbf{n}_0 = (\sin\chi, 0, \cos\chi). \tag{C5}$$

Now we introduce new unknown vectors Y_l via $Y_l = \check{D}\Psi_l$, where

$$\check{D} = \frac{1+\check{\tau}_z}{2} - i\check{\sigma}_y\frac{1-\check{\tau}_z}{2}. \tag{C6}$$

Multiplying Eq. (C1) from the left by $\check{D}\check{\tau}_z$, we obtain

$$\check{\tau}_z\left[\frac{\cot\alpha_\uparrow+\cot\alpha_\downarrow}{2} + \frac{\cot\alpha_\uparrow-\cot\alpha_\downarrow}{2}(\check{\sigma}_z\cos\chi+\check{\sigma}_x\sin\chi)\right]Y_l - \sum_n\left[\begin{pmatrix} g(l-n) & 0 \\ 0 & -g^*(l-n)\end{pmatrix}_N + i\check{\sigma}_y\begin{pmatrix} 0 & f^{\dagger *}(l-n) \\ -f^\dagger(l-n) & 0\end{pmatrix}_N\right] \times\left[\cos\left(\varphi\frac{l-n}{2}\right) + i\check{\tau}_z\check{\sigma}_z\sin\left(\varphi\frac{l-n}{2}\right)\right]Y_n = \epsilon Y_l, \tag{C7}$$

where ϵ is an effective energy, which we have to set equal to zero in accordance with Eq. (C1). Now one can check that the set of equations (C7) with different l define the coefficients of the Bogoliubov transformation that diagonalizes the effective Hamiltonian

$$\hat{H}_{\text{eff}} = \sum_{l,n,\alpha,\beta}\hat{a}^\dagger_{l\alpha}t_{\alpha\beta}(l-n)\hat{a}_{n\beta} + \frac{1}{2}\sum_{l,n,\alpha,\beta}[\hat{a}^\dagger_{l\alpha}\Delta_{\alpha\beta}(l-n)\hat{a}^\dagger_{n\beta} + \hat{a}_{n\beta}\Delta^*_{\alpha\beta}(l-n)\hat{a}_{l\alpha}], \tag{C8}$$

with the 2×2 matrices $\check{t}(l)$ and $\check{\Delta}(l)$ given by

$$\check{t}(l) = \begin{cases} \frac{\cot\alpha_\uparrow+\cot\alpha_\downarrow}{2} - g(0) + \frac{\cot\alpha_\uparrow-\cot\alpha_\downarrow}{2}(\check{\sigma}_z\cos\chi+\check{\sigma}_x\sin\chi) & \text{for} \quad l=0, \\ -g(l)e^{i\varphi l\hat{\sigma}_z/2} & \text{for} \quad l\neq 0, \end{cases} \tag{C9}$$

$$\check{\Delta}(l) = f^{\dagger *}(l)\begin{pmatrix} 0 & -e^{-i\varphi l/2} \\ e^{i\varphi l/2} & 0\end{pmatrix}. \tag{C10}$$

Here, $\hat{a}^\dagger_{l\alpha}$ and $\hat{a}_{l\alpha}$ are fermionic creation and annihilation operators, respectively, and α is a spin index. The fermionic operators satisfy standard commutation relations:

$$\hat{a}_{l\alpha}\hat{a}_{n\beta} + \hat{a}_{n\beta}\hat{a}_{l\alpha} = 0, \tag{C11}$$

$$\hat{a}^\dagger_{l\alpha}\hat{a}_{n\beta} + \hat{a}_{n\beta}\hat{a}^\dagger_{l\alpha} = \delta_{ln}\delta_{\alpha\beta}. \tag{C12}$$

The fermionic annihilation operators $\hat{b}$ that diagonalize the Hamiltonian (C8) have the form

$$\hat{b} = \sum_l(\hat{a}_{l\uparrow}, \hat{a}_{l\downarrow}, \hat{a}^\dagger_{l\uparrow}, \hat{a}^\dagger_{l\downarrow})Y^*_l, \tag{C13}$$

where the vectors Y_l satisfy Eq. (C7) with some real energy ϵ. It should be noted that the Hamiltonian $\hat{H}_{\text{eff}}$ formally corresponds to a Kitaev chain with two fermionic sites per unit cell.

Next, acting along the lines of Kitaev, the effective Hamiltonian should be written in terms of the Majorana operators

$$\hat{c}^{(1)}_{l\alpha} = \hat{a}_{l\alpha} + \hat{a}^\dagger_{l\alpha}, \qquad \hat{c}^{(2)}_{l\alpha} = \frac{\hat{a}_{l\alpha} - \hat{a}^\dagger_{l\alpha}}{i}. \tag{C14}$$

The result is

$$\hat{H}_{\text{eff}} = \frac{i}{4}\sum_{l,n}\sum_{\alpha,\beta=\uparrow,\downarrow}\sum_{i,j=1}^{2}B^{(ij)}_{\alpha\beta}(n-l)\hat{c}^{(i)}_{l\alpha}\hat{c}^{(j)}_{n\beta} + \text{const}, \tag{C15}$$

The coefficients here satisfy the relations

$$B^{(ij)}_{\alpha\beta}(l) = B^{(ij)*}_{\alpha\beta}(l), \qquad B^{(ij)}_{\alpha\beta}(l) = -B^{(ji)}_{\beta\alpha}(-l), \tag{C16}$$

and they are explicitly given by the formulas

$$B^{(11)}_{\uparrow\uparrow}(l) = B^{(22)}_{\uparrow\uparrow}(l) = -\tfrac{i}{2}[g(l)e^{il\varphi/2} - g^*(l)e^{-il\varphi/2}], \tag{C17}$$

$$B^{(11)}_{\downarrow\downarrow}(l) = B^{(22)}_{\downarrow\downarrow}(l) = -\tfrac{i}{2}[g(l)e^{-il\varphi/2} - g^*(l)e^{il\varphi/2}], \tag{C18}$$

$$B^{(12)}_{\uparrow\uparrow}(l) = -B^{(21)}_{\uparrow\uparrow}(l) = \left(\frac{\cot\alpha_\uparrow + \cot\alpha_\downarrow}{2} + \cos\chi\,\frac{\cot\alpha_\uparrow - \cot\alpha_\downarrow}{2}\right)\delta_{l0} - \frac{1}{2}[g(l)e^{il\varphi/2} + g^*(l)e^{-il\varphi/2}], \tag{C19}$$

$$B^{(12)}_{\downarrow\downarrow}(l) = -B^{(21)}_{\downarrow\downarrow}(l) = \left(\frac{\cot\alpha_\uparrow + \cot\alpha_\downarrow}{2} - \cos\chi\,\frac{\cot\alpha_\uparrow - \cot\alpha_\downarrow}{2}\right)\delta_{l0} - \frac{1}{2}[g(l)e^{-il\varphi/2} + g^*(l)e^{il\varphi/2}], \tag{C20}$$

$$B^{(11)}_{\uparrow\downarrow}(l) = -B^{(22)}_{\uparrow\downarrow}(l) = -\tfrac{i}{2}[f^\dagger(l)e^{-il\varphi/2} - f^{\dagger*}(l)e^{il\varphi/2}], \tag{C21}$$

$$B^{(11)}_{\downarrow\uparrow}(l) = -B^{(22)}_{\downarrow\uparrow}(l) = \tfrac{i}{2}[f^\dagger(l)e^{il\varphi/2} - f^{\dagger*}(l)e^{-il\varphi/2}], \tag{C22}$$

$$B^{(12)}_{\uparrow\downarrow}(l) = \delta_{l0}\frac{\cot\alpha_\uparrow - \cot\alpha_\downarrow}{2}\sin\chi - \frac{1}{2}[f^{\dagger*}(l)e^{il\varphi/2} + f^\dagger(l)e^{-il\varphi/2}], \tag{C23}$$

$$B^{(12)}_{\downarrow\uparrow}(l) = \delta_{l0}\frac{\cot\alpha_\uparrow - \cot\alpha_\downarrow}{2}\sin\chi + \frac{1}{2}[f^{\dagger*}(l)e^{-il\varphi/2} + f^\dagger(l)e^{il\varphi/2}], \tag{C24}$$

$$B^{(21)}_{\uparrow\downarrow}(l) = -\delta_{l0}\frac{\cot\alpha_\uparrow - \cot\alpha_\downarrow}{2}\sin\chi - \frac{1}{2}[f^{\dagger*}(l)e^{il\varphi/2} + f^\dagger(l)e^{-il\varphi/2}], \tag{C25}$$

$$B^{(21)}_{\downarrow\uparrow}(l) = -\delta_{l0}\frac{\cot\alpha_\uparrow - \cot\alpha_\downarrow}{2}\sin\chi + \frac{1}{2}[f^{\dagger*}(l)e^{-il\varphi/2} + f^\dagger(l)e^{il\varphi/2}]. \tag{C26}$$

The Majorana number $\mathcal{M}$ of a Kitaev chain is connected with the parity of the ground state of a closed chain with an even number of unit cells. An even ground state corresponds to a topologically trivial phase with $\mathcal{M} = 1$, and an odd ground state corresponds to a topologically nontrivial phase with $\mathcal{M} = -1$. One of the main findings of Kitaev [3] is the connection between the parity of the ground state and the Pfaffian of the Fourier-transformed matrix $B^{(ij)}_{\alpha\beta}(l)$. The Fourier transform is defined as follows:

$$\tilde{B}^{(ij)}_{\alpha\beta}(q) = \sum_{l=-\infty}^{+\infty} e^{iql} B^{(ij)}_{\alpha\beta}(l). \tag{C27}$$

Due to the properties (C16), the matrices $\tilde{B}(0)$ and $\tilde{B}(\pi)$ are skew-symmetric: $\tilde{B}^{(ij)}_{\alpha\beta}(q) = -\tilde{B}^{(ji)}_{\beta\alpha}(q)$, $q = 0, \pi$. The Majorana number equals

$$\mathcal{M} = \mathrm{sgn}[\mathrm{Pf}\tilde{B}(0)\mathrm{Pf}\tilde{B}(\pi)], \tag{C28}$$

where the Pfaffian is defined as follows:

$$\begin{aligned}\mathrm{Pf}\tilde{B}(q) = {}& \tilde{B}^{(12)}_{\uparrow\uparrow}(q)\tilde{B}^{(12)}_{\downarrow\downarrow}(q) + \tilde{B}^{(12)}_{\uparrow\downarrow}(q)\tilde{B}^{(21)}_{\uparrow\downarrow}(q) \\ & - \tilde{B}^{(11)}_{\uparrow\downarrow}(q)\tilde{B}^{(22)}_{\uparrow\downarrow}(q), \quad q = 0, \pi.\end{aligned} \tag{C29}$$

The results obtained so far in this Appendix are applicable to any translationally invariant nonmagnetic superconducting system with a helical chain of magnetic atoms lined up along the direction of translational invariance. Now we will specify the results for the case of our Josephson junction. Using Eqs. (18) and (19), we obtain

$$\tilde{B}^{(11)}_{\uparrow\uparrow}(0) = \tilde{B}^{(22)}_{\uparrow\uparrow}(0) = \tilde{B}^{(11)}_{\downarrow\downarrow}(0) = \tilde{B}^{(22)}_{\downarrow\downarrow}(0) = \tilde{B}^{(11)}_{\uparrow\downarrow}(0) = \tilde{B}^{(11)}_{\downarrow\uparrow}(0) = \tilde{B}^{(22)}_{\uparrow\downarrow}(0) = \tilde{B}^{(22)}_{\downarrow\uparrow}(0) = 0, \tag{C30}$$

$$\tilde{B}^{(12)}_{\uparrow\uparrow}(0) = -\tilde{B}^{(21)}_{\uparrow\uparrow}(0) = \cos\chi\,\tfrac{\cot\alpha_\uparrow - \cot\alpha_\downarrow}{2} - \tilde{l}\left(\tfrac{\varphi}{2}\right), \tag{C31}$$

$$\tilde{B}^{(12)}_{\downarrow\downarrow}(0) = -\tilde{B}^{(21)}_{\downarrow\downarrow}(0) = -\cos\chi\,\tfrac{\cot\alpha_\uparrow - \cot\alpha_\downarrow}{2} - \tilde{l}\left(\tfrac{\varphi}{2}\right), \tag{C32}$$

$$\tilde{B}^{(12)}_{\uparrow\downarrow}(0) = -\tilde{B}^{(21)}_{\downarrow\uparrow}(0) = \sin\chi\,\tfrac{\cot\alpha_\uparrow - \cot\alpha_\downarrow}{2} - \cos^{-1}\left(\tfrac{\theta}{2}\right)\tilde{h}\left(\tfrac{\varphi}{2}\right), \tag{C33}$$

$$\tilde{B}^{(21)}_{\uparrow\downarrow}(0) = -\tilde{B}^{(12)}_{\downarrow\uparrow}(0) = -\sin\chi\,\tfrac{\cot\alpha_\uparrow - \cot\alpha_\downarrow}{2} - \cos^{-1}\left(\tfrac{\theta}{2}\right)\tilde{h}\left(\tfrac{\varphi}{2}\right), \tag{C34}$$

To obtain $\tilde{B}(\pi)$, one should simply add 2π to φ in Eqs. (C30)–(C34). Finally, using Eqs. (C28) and (C29), we find that the Majorana number is given by Eq. (24).

APPENDIX D: EXPLICIT SOLUTION FOR A SIMPLIFIED TWO-BAND MODEL

In this Appendix, we will consider an approximate description of our system in terms of discrete BdG equations (26)—see Sec. IV B for details. These equations were initially derived by Pientka *et al.* [14] in the case of a bulk uniform superconductor, when the hopping and pairing amplitudes are given by

$$t(l)=\begin{cases}\epsilon_0 & \text{for } l=0\\ -\frac{\sin(al)}{al}\left(e^{il\varphi/2}\cos^2\frac{\chi}{2}+e^{-il\varphi/2}\sin^2\frac{\chi}{2}\right) & \text{for } l\neq 0\end{cases}, \tag{D1}$$

$$\Delta(l)=\begin{cases}0 & \text{for } l=0\\ i\frac{\cos(al)}{a|l|}\sin\chi\,\sin\left(l\frac{\varphi}{2}\right) & \text{for } l\neq 0\end{cases}, \tag{D2}$$

where $\epsilon_0=\cos(2\alpha_\uparrow)$ (for $\alpha_\uparrow\approx\pi/4$). In Eqs. (D1) and (D2) and further in this Appendix, the distance a between impurities is measured in units of k_F^{-1}. The model of Pientka *et al.* can be generalized for the case of a short Josephson junction considered in this paper, and for independent phases $\alpha_\uparrow$ and $\alpha_\downarrow$. Then, the quasiparticle wave function should be expanded in terms of the wave functions of generalized YSR states existing in short Josephson junctions [50]: we assume that Eq. (22) is approximately satisfied and seek the solution of Eq. (14) in the form

$$\Psi_l\approx\frac{1}{\sqrt{\tan\alpha_\uparrow-\tan\alpha_\downarrow}}\begin{pmatrix}\sqrt{\tan\alpha_\uparrow}\cos\frac{\chi}{2}\\ \sqrt{\tan\alpha_\uparrow}\sin\frac{\chi}{2}\\ \sqrt{-\tan\alpha_\downarrow}\cos\frac{\chi}{2}\\ \sqrt{-\tan\alpha_\downarrow}\sin\frac{\chi}{2}\end{pmatrix}u_l+\frac{1}{\sqrt{\tan\alpha_\uparrow-\tan\alpha_\downarrow}}\begin{pmatrix}-\sqrt{-\tan\alpha_\downarrow}\sin\frac{\chi}{2}\\ \sqrt{-\tan\alpha_\downarrow}\cos\frac{\chi}{2}\\ \sqrt{\tan\alpha_\uparrow}\sin\frac{\chi}{2}\\ -\sqrt{\tan\alpha_\uparrow}\cos\frac{\chi}{2}\end{pmatrix}v_l. \tag{D3}$$

The coefficients in Eq. (26) then take the form

$$t(l)=\begin{cases}\epsilon_0 & \text{for } l=0\\ \left[\frac{\cos(al)}{a|l|}(\tan\alpha_\uparrow+\tan\alpha_\downarrow)+2\frac{\sin(al)}{al}\right]\frac{\tan\alpha_\uparrow\tan\alpha_\downarrow}{\tan\alpha_\uparrow-\tan\alpha_\downarrow}\left(e^{il\varphi/2}\cos^2\frac{\chi}{2}+e^{-il\varphi/2}\sin^2\frac{\chi}{2}\right) & \text{for } l\neq 0\end{cases}, \tag{D4}$$

$$\Delta(l)=\begin{cases}0 & \text{for } l=0\\ -i\sin\chi\,\sin\left(l\frac{\varphi}{2}\right)\frac{\sqrt{-\tan\alpha_\uparrow\tan\alpha_\downarrow}}{\tan\alpha_\uparrow-\tan\alpha_\downarrow}\left[2\frac{\cos(al)}{a|l|}\tan\alpha_\uparrow\tan\alpha_\downarrow+\frac{\sin(al)}{al}(\tan\alpha_\uparrow+\tan\alpha_\downarrow)\right] & \text{for } l\neq 0\end{cases}, \tag{D5}$$

$$\epsilon_0=\frac{\cos^2\frac{\theta}{2}+\tan\alpha_\uparrow\tan\alpha_\downarrow}{\tan\alpha_\uparrow-\tan\alpha_\downarrow}. \tag{D6}$$

The described above models are applicable when $|\epsilon_0|\ll\cos(\theta/2)$.

If we are dealing with a semi-infinite impurity chain, such that $l=0,1\ldots$, Eq. (26) becomes a discrete vector Wiener-Hopf equation [64]. The general solution of such equations is not known, however, for $\chi=\pi/2$ our equation can be solved analytically. This case is somewhat special: if we introduce a set of unknown coefficients $u_l'=e^{-i\pi/4}u_l$ and $v_l'=e^{i\pi/4}v_l$, we obtain Eq. (26) with real coefficients $t(l)$ and $\Delta(l)$. This results in an effective time-reversal symmetry, so that our system falls into the BDI symmetry class [65].

To find the wave function of the MZM, we put $\epsilon=0$ and introduce a new set of unknown coefficients s_m and w_m:

$$\begin{pmatrix}u_m\\ v_m\end{pmatrix}=\begin{pmatrix}1 & 1\\ i & -i\end{pmatrix}\begin{pmatrix}s_m\\ w_m\end{pmatrix}. \tag{D7}$$

The equations for s_m and w_m decouple:

$$\sum_{m=0}^{\infty}Q_{l-m}s_m=0,\qquad l=0,1\ldots, \tag{D8}$$

$$\sum_{m=0}^{\infty}\tilde{Q}_{l-m}w_m=0,\qquad l=0,1\ldots, \tag{D9}$$

where

$$Q_l=\tfrac{1}{2}[t(l)+t(-l)+i\Delta(l)+i\Delta^*(-l)]=t(l)+i\Delta(l), \tag{D10}$$

$$\tilde{Q}_l=\tfrac{1}{2}[t(l)+t(-l)-i\Delta(l)-i\Delta^*(-l)]=t(l)-i\Delta(l). \tag{D11}$$

Equations (D8) and (D9) are scalar Wiener-Hopf equations, which can be solved analytically in the general case. To solve Eq. (D8), we first extend it to negative l:

$$\sum_{m=0}^{\infty}Q_{l-m}s_m=p_l,\qquad l=-1,-2\ldots, \tag{D12}$$

where p_l are unknown coefficients. Next, we apply a Z transform: we multiply Eqs. (D8) and (D12) by ζ^l, where ζ is a complex variable, and sum over l to obtain

$$Q(\zeta)s(\zeta)=p(\zeta), \tag{D13}$$

where

$$Q(\zeta)=\sum_{l=-\infty}^{+\infty}Q_l\zeta^l, \tag{D14}$$

$$s(\zeta)=\sum_{l=0}^{+\infty}s_l\zeta^l, \tag{D15}$$

$$p(\zeta) = \sum_{l=-\infty}^{-1} p_l \zeta^l. \tag{D16}$$

If we are seeking a physical solution of our equations corresponding to a boundary state, then $s_l \to 0$ when $l \to \infty$. This means that $s(\zeta)$ is regular for $|\zeta| < 1$. If we additionally assume that it is regular for $|\zeta| \leqslant 1$, $p(\zeta)$ is regular for $|\zeta| \geqslant 1$, and $Q(\zeta)$ together with $Q^{-1}(\zeta)$ are regular in the vicinity of the circle $|\zeta| = 1$, Eq. (D13) becomes a Riemann boundary value problem with unknown functions $s(\zeta)$ and $p(\zeta)$. The solution of this problem has been obtained by Gakhov [64,66]. As a first step of this solution, the function $Q(\zeta)$ should be factorized:

$$Q(\zeta) = Q_-(\zeta)\zeta^\kappa Q_+(\zeta), \tag{D17}$$

where $Q_+(\zeta)$ and $Q_+^{-1}(\zeta)$ are regular for $|\zeta| \leqslant 1$, $Q_-(\zeta)$ and $Q_-^{-1}(\zeta)$ are regular for $|\zeta| \geqslant 1$, and κ is an integer, which is called the Cauchy index (winding number) of $Q(\zeta)$. It is given by

$$\kappa = \frac{1}{2\pi} \oint_{|\zeta|=1} d(\arg Q(\zeta)). \tag{D18}$$

The function $\ln(Q(\zeta)\zeta^{-\kappa})$ is regular in the vicinity of the circle $|\zeta| = 1$. Then, we may put

$$Q_+(\zeta) = \exp\left(\frac{1}{2\pi i} \oint_{|t|=1} \frac{\ln(Q(t)t^{-\kappa})}{t-\zeta} dt\right) \tag{D19}$$

for $|\zeta| < 1$, and

$$Q_-(\zeta) = \exp\left(-\frac{1}{2\pi i} \oint_{|t|=1} \frac{\ln(Q(t)t^{-\kappa})}{t-\zeta} dt\right) \tag{D20}$$

for $|\zeta| > 1$. Here, the choice of the branch of the logarithms does not matter. Two cases are possible. If $\kappa \geqslant 0$, we rewrite Eq. (D13) in the form

$$\zeta^\kappa Q_+(\zeta)s(\zeta) = Q_-^{-1}(\zeta)p(\zeta). \tag{D21}$$

The Laurent series of the right-hand side of Eq. (D21) contains only negative powers of ζ, while the Laurent series of the left-hand side contains only non-negative powers of ζ, which means that both sides must be equal to zero. We find then that $s(\zeta) = 0$, $s_l = 0$ for all l, and Eq. (D8) has no physical solutions. The situation is different for $\kappa < 0$. In our particular case, if we use Eqs. (D1) and (D2), we may obtain $\kappa = -1$. Equation (D13) then can be rewritten in the form

$$Q_+(\zeta)s(\zeta) = \zeta Q_-^{-1}(\zeta)p(\zeta). \tag{D22}$$

The Laurent series of the right-hand side now contains only nonpositive powers of ζ, while the Laurent series of the left-hand side contains only non-negative powers of ζ, which means that both sides must be constant:

$$Q_+(\zeta)s(\zeta) = \zeta Q_-^{-1}(\zeta)p(\zeta) = \text{const}. \tag{D23}$$

To obtain a particular solution of Eq. (D13) we put const $= 1$, so that

$$s(\zeta) = Q_+^{-1}(\zeta). \tag{D24}$$

Finally, the solution of Eq. (D24) is given by

$$s_l = \frac{1}{2\pi i} \oint_{|\zeta|=1} \frac{d\zeta}{\zeta^{l+1} Q_+(\zeta)} = \frac{1}{2\pi} \int_0^{2\pi} \frac{e^{-il\beta} d\beta}{Q_+(e^{i\beta})}. \tag{D25}$$

To solve Eq. (D9), we have to factorize the function

$$\tilde{Q}(\zeta) = \sum_{l=-\infty}^{+\infty} \tilde{Q}_l \zeta^l. \tag{D26}$$

It follows form the relations $t(-l) = t(l)$ and $\Delta(-l) = -\Delta(l)$ that on the unit circle $\tilde{Q}(e^{i\beta}) = Q^*(e^{i\beta})$, which means that the sum of Cauchy indices of $Q(\zeta)$ and $\tilde{Q}(\zeta)$ equals zero.

Now we have to determine κ and $Q_+(\zeta)$ in our particular case. First, we perform the calculations using Eqs. (D1) and (D2) for the coefficients $t(l)$ and $\Delta(l)$. From Eq. (D14), we obtain

$$\begin{aligned} Q(\zeta) = \epsilon_0 + \frac{i}{2a}\Big[&\ln\left(1 - \exp\left(-i\left(\frac{\varphi}{2} + a\right) - \eta^+\right)\zeta\right) - \ln\left(1 - \exp\left(i\left(\frac{\varphi}{2} + a\right) - \eta^+\right)\zeta\right) \\ &+ \ln\left(1 - \exp\left(i\left(\frac{\varphi}{2} - a\right) - \eta^+\right)\zeta^{-1}\right) - \ln\left(1 - \exp\left(i\left(a - \frac{\varphi}{2}\right) - \eta^+\right)\zeta^{-1}\right)\Big]. \end{aligned} \tag{D27}$$

Here, the function $\ln(1-\zeta)$ is assumed regular for $|\zeta| < 1$, and $\ln(1) = 0$. On the unit circle

$$\begin{aligned} Q(e^{i\beta}) = \epsilon_0 + \frac{i}{2a}\Big[&\frac{1}{2}\ln\left(2 - 2\cos\left(\beta - \frac{\varphi}{2} - a\right)\right) + \frac{1}{2}\ln\left(2 - 2\cos\left(\frac{\varphi}{2} - a - \beta\right)\right) \\ &- \frac{1}{2}\ln\left(2 - 2\cos\left(\beta + \frac{\varphi}{2} + a\right)\right) - \frac{1}{2}\ln\left(2 - 2\cos\left(a - \frac{\varphi}{2} - \beta\right)\right) - 2ia \\ &+ \pi i\left(\left\lfloor \frac{a + \frac{\varphi}{2} + \beta}{2\pi} \right\rfloor + \left\lfloor \frac{a - \frac{\varphi}{2} - \beta}{2\pi} \right\rfloor - \left\lfloor \frac{\beta - \frac{\varphi}{2} - a}{2\pi} \right\rfloor - \left\lfloor \frac{\frac{\varphi}{2} - a - \beta}{2\pi} \right\rfloor\right)\Big], \end{aligned} \tag{D28}$$

It follows from Eqs. (D27) and (D28) that $Q(1)$ and $Q(-1)$ are real. One can also derive from Eq. (D28) that for $Q(1)Q(-1) > 1$ the Cauchy index equals either equals zero or is undefined, because $Q(\zeta)$ vanishes somewhere on the unit circle. When

$$Q(1)Q(-1) < 0, \tag{D29}$$

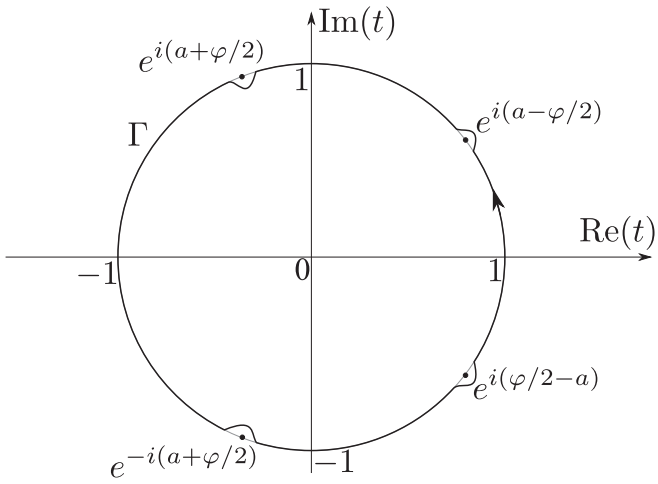

FIG. 6. Deformed integration contour for the calculation of κ, $Q_+(\zeta)$ and $Q_-(\zeta)$.

we obtain either $\kappa = 1$ or $\kappa = -1$, which means that either Eq. (D8) or Eq. (D9) has a nontrivial solution, indicating that our system is in a topologically nontrivial state. The only exception is the case $Q(1) + Q(-1) = 0$ when $Q(\zeta) = 0$ somewhere on the unit circle. This corresponds to a switching point, where the bulk spectrum of the chain is gapless, and κ changes its sign.

When factorizing the function $Q(\zeta)$, we may put $\eta^+ = 0$, and integrate along the deformed contour Γ in Fig. 6 instead of the unit circle in Eqs. (D18)–(D20). Then, the singularities of $Q(\zeta)$ are logarithmic branch points located at $\zeta = \exp(\pm i(a + \varphi/2))$, and the singularities of $Q_-(\zeta)$ are logarithmic branch points located at $\zeta = \exp(\pm i(a - \varphi/2))$. We assume here that the singularities do not merge. The case $\exp(\pm i(a - \varphi/2)) = 1$ has been studied in Ref. [51].

Consider a set of parameters such that $\kappa = -1$. An exemplary set is $\epsilon_0 = 0$, $\varphi = \pi/2$, and $a = 2\pi n - \pi/3$, where n is a large positive integer ($a \gg 1$ is an applicability condition for Eq. (26)). The explicit solution for the coefficients s_l is given by Eq. (D25). Now we will be mainly interested in the asymptotic behavior of s_l in the limit of large l. It follows from Eq. (D25) that s_l can be written in the form of a Fourier integral, whose behavior in the limit $l \to \infty$ is determined by the singularities of $Q_+^{-1}(e^{i\beta})$ [67]. These singularities were found above. Then, since $Q_+(\zeta) = Q(\zeta)Q_-^{-1}(\zeta)\zeta$, using Eq. (D27) we obtain from Eq. (D25) that

$$s_l \approx \frac{1}{2\pi i}\oint_{|\zeta|=1} 2ai\left[\frac{\exp\left(i\left(\frac{\varphi}{2}+a\right)\right)Q_-\left(\exp\left(-i\left(\frac{\varphi}{2}+a\right)\right)\right)}{\ln\left(1-\exp\left(i\left(\frac{\varphi}{2}+a\right)\right)\zeta\right)} - \frac{\exp\left(-i\left(\frac{\varphi}{2}+a\right)\right)Q_-\left(\exp\left(i\left(\frac{\varphi}{2}+a\right)\right)\right)}{\ln\left(1-\exp\left(-i\left(\frac{\varphi}{2}+a\right)\right)\zeta\right)}\right]\frac{d\zeta}{\zeta^{l+1}}$$
$$= \frac{a}{\pi}\left[\exp\left(i(l+1)\left(\frac{\varphi}{2}+a\right)\right)Q_-\left(\exp\left(-i\left(\frac{\varphi}{2}+a\right)\right)\right) - \exp\left(-i(l+1)\left(\frac{\varphi}{2}+a\right)\right)Q_-\left(\exp\left(i\left(\frac{\varphi}{2}+a\right)\right)\right)\right]I_l, \quad \text{(D30)}$$

where

$$I_l = \oint_{|\zeta|=1} \frac{d\zeta}{\ln(1-\zeta)\zeta^{l+1}}. \quad \text{(D31)}$$

The integration contour here can be deformed, so that

$$I_l = \int_{1-i\infty}^{1+i\infty} \frac{d\zeta}{\ln(1-\zeta)\zeta^{l+1}} - \int_{-d-i\infty}^{-d+i\infty} \frac{d\zeta}{\ln(1-\zeta)\zeta^{l+1}}, \quad \text{(D32)}$$

where d is an arbitrary positive number. Since d can be taken arbitrary large, the second integral in the right-hand side of Eq. (D32) vanishes. The contour in the first integral in the right-hand side can be deformed in such a way that it will go around the branch cut of the logarithm:

$$I_l = \int_1^\infty \left[\frac{1}{\ln(\zeta-1)-i\pi} - \frac{1}{\ln(\zeta-1)+i\pi}\right]\frac{d\zeta}{\zeta^{l+1}}$$
$$= 2\pi i\int_1^\infty \frac{d\zeta}{\zeta^{l+1}[\ln^2(\zeta-1)+\pi^2]}, \quad \text{(D33)}$$

where the logarithm is real-valued. Next, we introduce the integration variable $t = l\ln\zeta$:

$$I_l = \frac{2\pi i}{l}\int_0^\infty \frac{e^{-t}dt}{\ln^2(e^{t/l}-1)+\pi^2}. \quad \text{(D34)}$$

In the limit of large l, in the denominator we can put $e^{t/l} - 1 \approx t/l$. The final transformations look as follows:

$$I_l \approx \frac{2\pi i}{l}\int_0^\infty \frac{e^{-t}dt}{\ln^2\frac{t}{l}+\pi^2}$$
$$= \frac{2\pi i}{l\ln^2 l}\int_0^\infty \frac{e^{-t}dt}{\left(1-\frac{\ln t}{\ln l}\right)^2+\frac{\pi^2}{\ln^2 l}}$$
$$\approx \frac{2\pi i}{l\ln^2 l}\int_0^\infty e^{-t}dt = \frac{2\pi i}{l\ln^2 l}. \quad \text{(D35)}$$

Combining Eqs. (D7), (D30), and (D35), we obtain

$$\begin{pmatrix} u_l \\ v_l \end{pmatrix} = \frac{2ai}{l\ln^2 l}\Big[\exp\Big(i(l+1)\Big(\frac{\varphi}{2}+a\Big)\Big)Q_-\Big(\exp\Big(-i\Big(\frac{\varphi}{2}+a\Big)\Big)\Big) - \exp\Big(-i(l+1)\Big(\frac{\varphi}{2}+a\Big)\Big)Q_-\Big(\exp\Big(i\Big(\frac{\varphi}{2}+a\Big)\Big)\Big)\Big]\begin{pmatrix}1\\ i\end{pmatrix}. \tag{D36}$$

In the case $\kappa = 1$, Eq. (D9) has a nontrivial solution, which can be found in a similar way.

Finally, we analyze the more general situation, when the hopping and pairing amplitudes are given by Eqs. (D4) and (D5). The function $Q(\zeta)$ takes the form

$$\begin{aligned} Q(\zeta) = \epsilon_0 - \frac{\rho}{4a(\tan\alpha_\uparrow - \tan\alpha_\downarrow)}\Big\{&(\rho+1)(2i\rho-\tau)\Big[\ln\Big(1-\exp\Big(i\Big(a+\frac{\varphi}{2}\Big)\Big)\zeta\Big)+\ln\Big(1-\exp\Big(i\Big(a-\frac{\varphi}{2}\Big)\Big)\zeta^{-1}\Big)\Big]\\ &+(1-\rho)(2i\rho+\tau)\Big[\ln\Big(1-\exp\Big(i\Big(a-\frac{\varphi}{2}\Big)\Big)\zeta\Big)+\ln\Big(1-\exp\Big(i\Big(a+\frac{\varphi}{2}\Big)\Big)\zeta^{-1}\Big)\Big]\\ &+(1-\rho)(\tau-2i\rho)\Big[\ln\Big(1-\exp\Big(i\Big(\frac{\varphi}{2}-a\Big)\Big)\zeta\Big)+\ln\Big(1-\exp\Big(-i\Big(a+\frac{\varphi}{2}\Big)\Big)\zeta^{-1}\Big)\Big]\\ &-(1+\rho)(\tau+2i\rho)\Big[\ln\Big(1-\exp\Big(-i\Big(\frac{\varphi}{2}+a\Big)\Big)\zeta\Big)+\ln\Big(1-\exp\Big(i\Big(\frac{\varphi}{2}-a\Big)\Big)\zeta^{-1}\Big)\Big]\Big\}, \end{aligned} \tag{D37}$$

where

$$\rho = \sqrt{-\tan\alpha_\uparrow\tan\alpha_\downarrow} = \cos\frac{\theta}{2}, \tag{D38}$$

$$\tau = \tan\alpha_\uparrow + \tan\alpha_\downarrow. \tag{D39}$$

The factors $e^{\pm\eta_+}$ in Eq. (D37) were omitted for brevity. We will not calculate the index κ here, assuming $\kappa = -1$. For $\rho = 1$ ($\theta = 0$) and arbitrary τ, the singularities of $Q_+(\zeta)$ are located at the same points as before, and the asymptotic behavior $s_l \sim 1/(l\ln^2 l)$ can be obtained in the same way as above. However, for $\rho \neq 1$ the situation is qualitatively different: the function $Q(\zeta)$ has 8 logarithmic singularities instead of 4, and in the limit $\eta^+ \to 0$ the singularities merge in pairs on the unit circle. To calculate s_l in this case, we use a deformed integration contour $\tilde\Gamma$ shown in Fig. 7 instead of the unit circle in Eq. (D25). This contour consists of four segments—Γ_1, Γ_2, Γ_3, and Γ_4—enclosing the branch cuts of $Q(\zeta)$, and of four segments denoted as Γ_{out} lying on the circle $|\zeta| = R$. Here, $R - 1 \ll 1$, and $Q(\zeta)$ must have no zeros between the contours $|\zeta| = 1$ and $\tilde\Gamma$. We can break s_l down into five terms:

$$s_l = \sum_{i=1}^{4} s_l^{(i)} + s_l^{(\text{out})}, \tag{D40}$$

where

$$s_l^{(i)} = \frac{1}{2\pi i}\int_{\Gamma_i}\frac{d\zeta}{\zeta^{l+1}Q_+(\zeta)}, \tag{D41}$$

$$s_l^{(\text{out})} = \frac{1}{2\pi i}\int_{\Gamma_{\text{out}}}\frac{d\zeta}{\zeta^{l+1}Q_+(\zeta)} = \frac{1}{2\pi R^l}\int_0^{2\pi}\frac{e^{-il\beta}d\beta}{Q_+(Re^{i\beta})}. \tag{D42}$$

The integrand in the right-hand side of Eq. (D42) is discontinuous due to the presence of branch cuts. The corresponding integral tends to zero when $l \to \infty$ by virtue of the Riemann-Lebesgue lemma. Hence, $s_l^{(\text{out})}$ is exponentially small in the limit $l \to \infty$ due to the presence of the factor R^{-l} in Eq. (D42).

Let us consider the term $s_l^{(1)}$. Introducing the integration variable $\zeta_1 = \exp(-i(a+\varphi/2))\zeta$, we obtain

$$s_l^{(1)} = \frac{e^{-il(a+\varphi/2)}}{2\pi i}\int_1^R\frac{d\zeta_1}{\zeta_1^{l+1}}\Big[\frac{1}{\bar Q_+(\zeta_1+i0)} - \frac{1}{\bar Q_+(\zeta_1-i0)}\Big], \tag{D43}$$

where

$$\bar Q_+(\zeta_1) = Q_+(\zeta_1 e^{i(a+\varphi/2)}). \tag{D44}$$

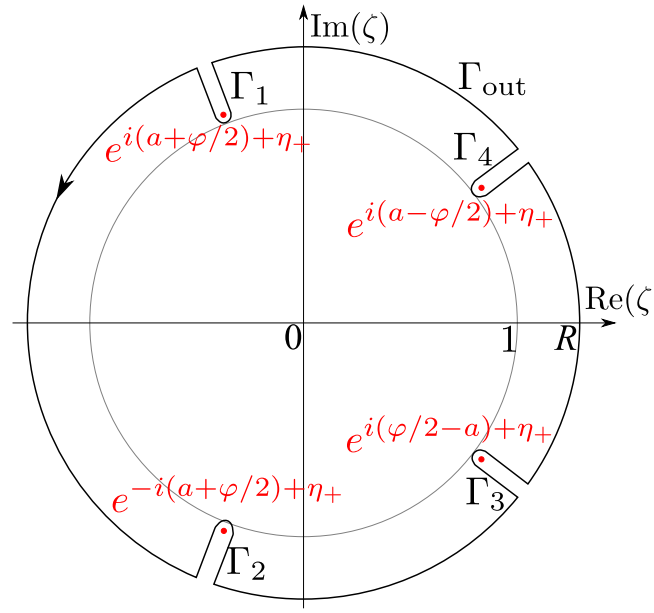

FIG. 7. Integration contour $\tilde\Gamma$ used to calculate $Q_+(\zeta)$ and s_l when $Q(\zeta)$ is given by Eq. (D37).

Now we need to determine the behavior of $\bar{Q}_+(\zeta_1)$ for ζ_1 close to 1. To do this, first, in Eq. (D19) we integrate along the deformed contour $\tilde{\Gamma}$ (Fig. 7) instead of the unit circle, and we write $Q_+(\zeta)$ in the form

$$Q_+(\zeta) = Q_+^{(R)}(\zeta) Q_+^{(1)}(\zeta), \tag{D45}$$

where

$$Q_+^{(R)}(\zeta) = \exp\left(\frac{1}{2\pi i}\int_{\tilde{\Gamma}\setminus\Gamma_1} \frac{\ln(Q(t)t)}{t-\zeta} dt\right), \tag{D46}$$

$$Q_+^{(1)}(\zeta) = \exp\left(\frac{1}{2\pi i}\int_{\Gamma_1} \frac{\ln(Q(t)t)}{t-\zeta} dt\right). \tag{D47}$$

The function $Q_+^{(R)}(\zeta)$ is regular for $\zeta = \exp(-i(a+\varphi/2))$, and hence $\bar{Q}_+(\zeta_1)$ for $\zeta_1 \approx 1$ takes the form

$$\bar{Q}_+(\zeta_1) \approx Q_+^{(R)}(e^{i(a+\varphi/2)}) \exp\left(\frac{1}{2\pi i}\int_1^R \frac{\ln\left(\frac{\bar{Q}(t_1+i0)}{\bar{Q}(t_1-i0)}\right)}{t_1-\zeta_1} dt_1\right), \tag{D48}$$

where we use the integration variable $t_1 = \exp(-i(a+\varphi/2))t$, and

$$\bar{Q}(t_1) = Q(t_1 e^{i(a+\varphi/2)}). \tag{D49}$$

Next, for $t_1 \in (1, R)$ we obtain using Eq. (D37)

$$\begin{aligned}\ln\left(\frac{\bar{Q}(t_1+i0)}{\bar{Q}(t_1-i0)}\right) &= \ln\left(1+\frac{\bar{Q}(t_1+i0)-\bar{Q}(t_1-i0)}{\bar{Q}(t_1-i0)}\right) \approx \frac{\bar{Q}(t_1+i0)-\bar{Q}(t_1-i0)}{\bar{Q}(t_1-i0)} \\ &\approx \frac{-2\pi i(1+\rho)}{\ln(1-t_1-i0)(1+\rho)-(1-\rho)\ln(1-t_1^{-1})} \approx \frac{-2\pi i(1+\rho)}{2\rho\ln(t_1-1)}.\end{aligned} \tag{D50}$$

Then, Eq. (D48) yields

$$\bar{Q}_+(\zeta_1) \approx Q_+^{(R)}(e^{i(a+\varphi/2)}) \left[\exp\left(-\int_1^R \frac{dt_1}{(t_1-\zeta_1)\ln(t_1-1)}\right)\right]^{\frac{1+\rho}{2\rho}}. \tag{D51}$$

It follows from the considerations of the simplified model with $Q(\zeta)$ given by Eq. (D27) that for $\rho = 1$ we have $\bar{Q}(\zeta_1) \propto \ln(1-\zeta_1)$ for $\zeta_1 \approx 1$. Hence, for an arbitrary value of ρ we have

$$\bar{Q}_+(\zeta_1) \approx C_1[\ln(1-\zeta_1)]^{\frac{1+\rho}{2\rho}}, \tag{D52}$$

where C_1 is some constant. To transform Eq. (D43), we note that in the limit of large l the main contribution to the integral in the right-hand side comes from ζ_1 very close to 1. We have then

$$\begin{aligned}s_l^{(1)} &\approx \frac{e^{-il(a+\varphi/2)}}{2\pi i C_1}\int_1^\infty \frac{d\zeta_1}{\zeta_1^{l+1}}\left\{\frac{1}{[\ln(\zeta_1-1)-i\pi]^{\frac{1+\rho}{2\rho}}} - \frac{1}{[\ln(\zeta_1-1)+i\pi]^{\frac{1+\rho}{2\rho}}}\right\} \\ &= \frac{e^{-il(a+\varphi/2)}}{2\pi i C_1}\int_1^\infty \frac{d\zeta_1}{\zeta_1^{l+1}[\ln(\zeta_1-1)]^{\frac{1+\rho}{2\rho}}}\left\{\frac{1}{\left[1-\frac{i\pi}{\ln(\zeta_1-1)}\right]^{\frac{1+\rho}{2\rho}}} - \frac{1}{\left[1+\frac{i\pi}{\ln(\zeta_1-1)}\right]^{\frac{1+\rho}{2\rho}}}\right\} \\ &\approx \frac{e^{-il(a+\varphi/2)}(1+\rho)}{2\rho C_1}\int_1^\infty \frac{d\zeta_1}{\zeta_1^{l+1}[\ln(\zeta_1-1)]^{\frac{1+3\rho}{2\rho}}}.\end{aligned} \tag{D53}$$

Further transformations are similar to those used in Eqs. (D33)–(D35). We obtain

$$s_l^{(1)} = \frac{\tilde{C}_1 e^{-il(a+\varphi/2)}}{l(\ln l)^{\frac{1+3\rho}{2\rho}}}, \tag{D54}$$

where $\tilde{C}_1$ is a constant. If we calculate $s_l^{(2)}$, we may find that $s_l^{(2)} = s_l^{(1)*}$, which is related to the fact that s_l is real. For $s_l^{(3)}$ and $s_l^{(4)}$, we obtain

$$s_l^{(3)} = \frac{\tilde{C}_3 e^{-il(\varphi/2-a)}}{l(\ln l)^{\frac{3\rho-1}{2\rho}}}, \qquad s_l^{(4)} = s_l^{(3)*}, \tag{D55}$$

where $\tilde{C}_3$ is one more constant. For $\rho = 1$ $\tilde{C}_3 = 0$, but otherwise for sufficiently large l the contributions $s_l^{(3)}$ and $s_l^{(4)}$ to s_l dominate. Thus, for $\theta \neq 0$ in the limit $l \to \infty$, we have

$$\begin{pmatrix} u_l \\ v_l \end{pmatrix} = \frac{2\mathrm{Re}(\tilde{C}_3 e^{-il(\varphi/2-a)})}{l(\ln l)^{\frac{3\rho-1}{2\rho}}}\begin{pmatrix} 1 \\ i \end{pmatrix}. \tag{D56}$$

[1] C. Nayak, S. H. Simon, A. Stern, M. Freedman, and S. Das Sarma, Non-Abelian anyons and topological quantum computation, Rev. Mod. Phys. **80**, 1083 (2008).

[2] V. Lahtinen and J. K. Pachos, A Short Introduction to Topological Quantum Computation, SciPost Phys. **3**, 021 (2017).

[3] A. Y. Kitaev, Unpaired Majorana fermions in quantum wires, Phys. Usp. **44**, 131 (2001).

[4] R. M. Lutchyn, J. D. Sau, and S. Das Sarma, Majorana Fermions and a Topological Phase Transition in Semiconductor-Superconductor Heterostructures, Phys. Rev. Lett. **105**, 077001 (2010).

[5] Y. Oreg, G. Refael, and F. von Oppen, Helical Liquids and Majorana Bound States in Quantum Wires, Phys. Rev. Lett. **105**, 177002 (2010).

[6] R. M. Lutchyn, E. P. A. M. Bakkers, L. P. Kouwenhoven, P. Krogstrup, C. M. Marcus, and Y. Oreg, Majorana zero modes in superconductor-semiconductor heterostructures, Nat. Rev. Mater. **3**, 52 (2018).

[7] M. Kjaergaard, K. Wölms, and K. Flensberg, Majorana fermions in superconducting nanowires without spin-orbit coupling, Phys. Rev. B **85**, 020503(R) (2012).

[8] I. Martin and A. F. Morpurgo, Majorana fermions in superconducting helical magnets, Phys. Rev. B **85**, 144505 (2012).

[9] T.-P. Choy, J. M. Edge, A. R. Akhmerov, and C. W. J. Beenakker, Majorana fermions emerging from magnetic nanoparticles on a superconductor without spin-orbit coupling, Phys. Rev. B **84**, 195442 (2011).

[10] S. Nadj-Perge, I. K. Drozdov, B. A. Bernevig, and A. Yazdani, Proposal for realizing Majorana fermions in chains of magnetic atoms on a superconductor, Phys. Rev. B **88**, 020407(R) (2013).

[11] J. Klinovaja, P. Stano, A. Yazdani, and D. Loss, Topological Superconductivity and Majorana Fermions in RKKY Systems, Phys. Rev. Lett. **111**, 186805 (2013).

[12] B. Braunecker and P. Simon, Interplay between Classical Magnetic Moments and Superconductivity in Quantum One-Dimensional Conductors: Toward a Self-Sustained Topological Majorana Phase, Phys. Rev. Lett. **111**, 147202 (2013).

[13] M. M. Vazifeh and M. Franz, Self-Organized Topological State with Majorana Fermions, Phys. Rev. Lett. **111**, 206802 (2013).

[14] F. Pientka, L. I. Glazman, and F. von Oppen, Topological superconducting phase in helical Shiba chains, Phys. Rev. B **88**, 155420 (2013).

[15] J. Röntynen and T. Ojanen, Tuning topological superconductivity in helical Shiba chains by supercurrent, Phys. Rev. B **90**, 180503(R) (2014).

[16] Y. Kim, M. Cheng, B. Bauer, R. M. Lutchyn, and S. Das Sarma, Helical order in one-dimensional magnetic atom chains and possible emergence of Majorana bound states, Phys. Rev. B **90**, 060401(R) (2014).

[17] K. Pöyhönen, A. Westström, J. Röntynen, and T. Ojanen, Majorana states in helical Shiba chains and ladders, Phys. Rev. B **89**, 115109 (2014).

[18] A. Westström, K. Pöyhönen, and T. Ojanen, Topological properties of helical Shiba chains with general impurity strength and hybridization, Phys. Rev. B **91**, 064502 (2015).

[19] A. Westström, K. Pöyhönen, and T. Ojanen, Topological superconductivity and anti-Shiba states in disordered chains of magnetic adatoms, Phys. Rev. B **94**, 104519 (2016).

[20] S. Hoffman, J. Klinovaja, and D. Loss, Topological phases of inhomogeneous superconductivity, Phys. Rev. B **93**, 165418 (2016).

[21] G. M. Andolina and P. Simon, Topological properties of chains of magnetic impurities on a superconducting substrate: Interplay between the Shiba band and ferromagnetic wire limits, Phys. Rev. B **96**, 235411 (2017).

[22] I. Reis, D. J. J. Marchand, and M. Franz, Self-organized topological state in a magnetic chain on the surface of a superconductor, Phys. Rev. B **90**, 085124 (2014).

[23] W. Hu, R. T. Scalettar, and R. R. P. Singh, Interplay of magnetic order, pairing, and phase separation in a one-dimensional spin-fermion model, Phys. Rev. B **92**, 115133 (2015).

[24] M. Schecter, M. S. Rudner, and K. Flensberg, Spin-Lattice Order in One-Dimensional Conductors: Beyond the RKKY Effect, Phys. Rev. Lett. **114**, 247205 (2015).

[25] B. Braunecker and P. Simon, Self-stabilizing temperature-driven crossover between topological and nontopological ordered phases in one-dimensional conductors, Phys. Rev. B **92**, 241410(R) (2015).

[26] M. Schecter, K. Flensberg, M. H. Christensen, B. M. Andersen, and J. Paaske, Self-organized topological superconductivity in a Yu-Shiba-Rusinov chain, Phys. Rev. B **93**, 140503(R) (2016).

[27] M. H. Christensen, M. Schecter, K. Flensberg, B. M. Andersen, and J. Paaske, Spiral magnetic order and topological superconductivity in a chain of magnetic adatoms on a two-dimensional superconductor, Phys. Rev. B **94**, 144509 (2016).

[28] M. Menzel, Y. Mokrousov, R. Wieser, J. E. Bickel, E. Vedmedenko, S. Blügel, S. Heinze, K. von Bergmann, A. Kubetzka, and R. Wiesendanger, Information Transfer by Vector Spin Chirality in Finite Magnetic Chains, Phys. Rev. Lett. **108**, 197204 (2012).

[29] M. Menzel, A. Kubetzka, K. von Bergmann, and R. Wiesendanger, Parity Effects in 120° Spin Spirals, Phys. Rev. Lett. **112**, 047204 (2014).

[30] M. Steinbrecher, R. Rausch, K. T. That, J. Hermenau, A. A. Khajetoorians, M. Potthoff, R. Wiesendanger, and J. Wiebe, Non-collinear spin states in bottom-up fabricated atomic chains, Nat. Commun. **9**, 2853 (2018).

[31] H. Kim, A. Palacio-Morales, T. Posske, L. Rózsa, K. Palotás, L. Szunyogh, M. Thorwart, and R. Wiesendanger, Toward tailoring Majorana bound states in artificially constructed magnetic atom chains on elemental superconductors, Sci. Adv. **4**, eaar5251 (2018).

[32] J. Alicea, Y. Oreg, G. Refael, F. von Oppen, and M. P. A. Fisher, Non-Abelian statistics and topological quantum information processing in 1D wire networks, Nat. Phys. **7**, 412 (2011).

[33] B. Seradjeh and E. Grosfeld, Unpaired Majorana fermions in a layered topological superconductor, Phys. Rev. B **83**, 174521 (2011).

[34] A. Romito, J. Alicea, G. Refael, and F. von Oppen, Manipulating Majorana fermions using supercurrents, Phys. Rev. B **85**, 020502(R) (2012).

[35] X.-J. Liu and A. M. Lobos, Manipulating Majorana fermions in quantum nanowires with broken inversion symmetry, Phys. Rev. B **87**, 060504(R) (2013).

[36] P. Kotetes, Classification of engineered topological superconductors, New J. Phys. **15**, 105027 (2013).

[37] A. Heimes, P. Kotetes, and G. Schön, Majorana fermions from Shiba states in an antiferromagnetic chain on top of a superconductor, Phys. Rev. B **90**, 060507(R) (2014).
[38] P. Kotetes, Topological superconductivity in Rashba semiconductors without a Zeeman field, Phys. Rev. B **92**, 014514 (2015).
[39] M. Hell, M. Leijnse, and K. Flensberg, Two-Dimensional Platform for Networks of Majorana Bound States, Phys. Rev. Lett. **118**, 107701 (2017).
[40] F. Pientka, A. Keselman, E. Berg, A. Yacoby, A. Stern, and B. I. Halperin, Topological Superconductivity in a Planar Josephson Junction, Phys. Rev. X **7**, 021032 (2017).
[41] O. Dmytruk, M. Thakurathi, D. Loss, and J. Klinovaja, Majorana bound states in double nanowires with reduced Zeeman thresholds due to supercurrents, Phys. Rev. B **99**, 245416 (2019).
[42] A. Melo, S. Rubbert, and A. R. Akhmerov, Supercurrent-induced Majorana bound states in a planar geometry, SciPost Phys. **7**, 039 (2019).
[43] T. Laeven, B. Nijholt, M. Wimmer, and A. R. Akhmerov, Enhanced Proximity Effect in Zigzag-Shaped Majorana Josephson Junctions, Phys. Rev. Lett. **125**, 086802 (2020).
[44] O. Lesser, K. Flensberg, F. von Oppen, and Y. Oreg, Three-phase majorana zero modes at tiny magnetic fields, Phys. Rev. B **103**, L121116 (2021).
[45] O. Lesser, A. Saydjari, M. Wesson, A. Yacoby, and Y. Oreg, Phase-induced topological superconductivity in a planar heterostructure, Proc. Natl. Acad. Sci. U.S.A. **118**, e2107377118 (2021).
[46] O. Lesser and Y. Oreg, Majorana zero modes induced by superconducting phase bias, J. Phys. D: Appl. Phys. **55**, 164001 (2022).
[47] L. Yu, Bound state in superconductors with paramagnetic impurities, Acta Phys. Sin. **21**, 75 (1965).
[48] H. Shiba, Classical spins in superconductors, Prog. Theor. Phys. **40**, 435 (1968).
[49] A. I. Rusinov, On the theory of gapless superconductivity in alloys containing paramagnetic impurities, Sov. Phys. JETP **29**, 1101 (1969) [Zh. Eksp. Teor. Fiz. **56**, 2047 (1969)].
[50] A. A. Bespalov, Quasibound states in short SNS junctions with point defects, Phys. Rev. B **97**, 134504 (2018).
[51] F. Pientka, L. I. Glazman, and F. von Oppen, Unconventional topological phase transitions in helical Shiba chains, Phys. Rev. B **89**, 180505(R) (2014).
[52] K. K. Likharev, Superconducting weak links, Rev. Mod. Phys. **51**, 101 (1979).
[53] N. Kopnin, *Theory of Nonequilibrium Superconductivity*, International Series of Monographs on Physics (Clarendon Press, Oxford, 2001).
[54] M. R. Zirnbauer, Riemannian symmetric superspaces and their origin in random-matrix theory, J. Math. Phys. **37**, 4986 (1996).
[55] A. Altland and M. R. Zirnbauer, Nonstandard symmetry classes in mesoscopic normal-superconducting hybrid structures, Phys. Rev. B **55**, 1142 (1997).
[56] C.-K. Chiu, J. C. Y. Teo, A. P. Schnyder, and S. Ryu, Classification of topological quantum matter with symmetries, Rev. Mod. Phys. **88**, 035005 (2016).
[57] D. Vodola, L. Lepori, E. Ercolessi, A. V. Gorshkov, and G. Pupillo, Kitaev Chains with Long-Range Pairing, Phys. Rev. Lett. **113**, 156402 (2014).
[58] D. Vodola, L. Lepori, E. Ercolessi, and G. Pupillo, Long-range Ising and Kitaev models: Phases, correlations and edge modes, New J. Phys. **18**, 015001 (2015).
[59] S. B. Jäger, L. Dell'Anna, and G. Morigi, Edge states of the long-range Kitaev chain: An analytical study, Phys. Rev. B **102**, 035152 (2020).
[60] D. R. Smith and P. H. Keesom, Specific heat of rhenium between 0.15 and 4.0 k, Phys. Rev. B **1**, 188 (1970).
[61] J. Shabani, M. Kjaergaard, H. J. Suominen, Y. Kim, F. Nichele, K. Pakrouski, T. Stankevic, R. M. Lutchyn, P. Krogstrup, R. Feidenhans'l, S. Kraemer, C. Nayak, M. Troyer, C. M. Marcus, and C. J. Palmstrøm, Two-dimensional epitaxial superconductor-semiconductor heterostructures: A platform for topological superconducting networks, Phys. Rev. B **93**, 155402 (2016).
[62] A. Fornieri, A. M. Whiticar, F. Setiawan, E. Portolés, A. C. C. Drachmann, A. Keselman, S. Gronin, C. Thomas, T. Wang, R. Kallaher, G. C. Gardner, E. Berg, M. J. Manfra, A. Stern, C. M. Marcus, and F. Nichele, Evidence of topological superconductivity in planar Josephson junctions, Nature (London) **569**, 89 (2019).
[63] https://en.wikipedia.org/wiki/Quartic_equation.
[64] A. V. Kisil, I. D. Abrahams, G. Mishuris, and S. V. Rogosin, The Wiener-Hopf technique, its generalizations and applications: constructive and approximate methods, Proc. R. Soc. A **477**, 20210533 (2021).
[65] W. DeGottardi, M. Thakurathi, S. Vishveshwara, and D. Sen, Majorana fermions in superconducting wires: Effects of long-range hopping, broken time-reversal symmetry, and potential landscapes, Phys. Rev. B **88**, 165111 (2013).
[66] F. D. Gakhov, *Boundary Value Problems*, edited by I. N. Sneddon, Dover Books on Advanced Mathematics (Dover, New York, 1990).
[67] N. Bleistein and R. A. Handelsman, *Asymptotic Expansions of Integrals* (Dover, New York, 1986).